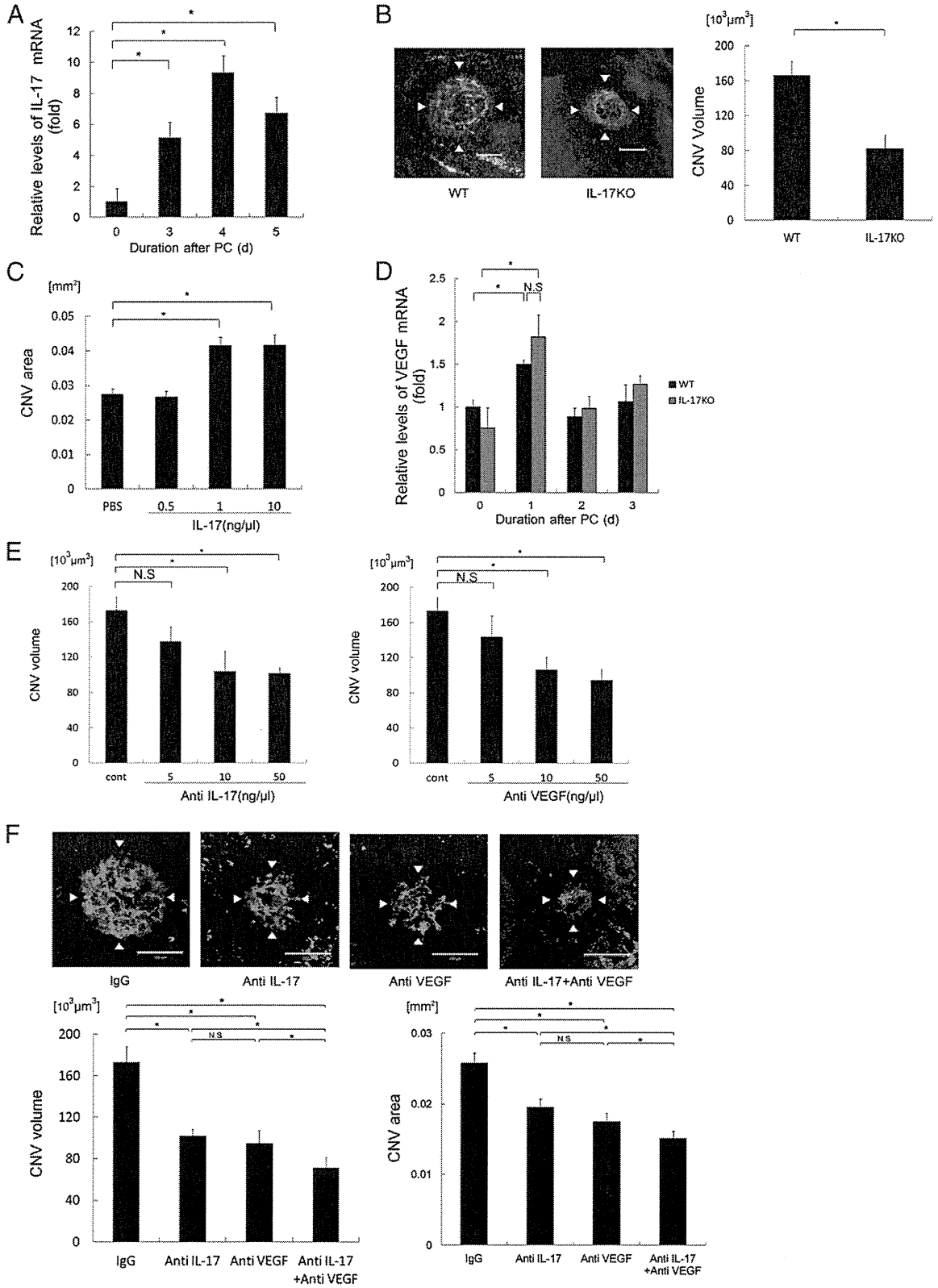

FIGURE 1. Angiogenic activity of IL-17 in CNV. (**A**)Total RNA was extracted from the eyes of WT mice on the indicated days after laser treatment ($n = 3$). *Il17a* mRNA levels were normalized to *HPRT* levels in each sample. (**B**) On day 7 after laser treatment, the sizes of CNV volumes were compared in WT mice and IL-17 KO mice ($n = 10–15$). Representative CNV lesions of choroidal flat mounts are shown. Arrowheads indicate stained CNV tissues. Scale bars, 100 μm. (**C**) rIL-17 (0.5, 1, or 10 ng/μl; 2 μl) was inoculated into the vitreous cavities of WT mice immediately after laser treatment ($n = 10–15$). On day 7 after laser treatment, the sizes of CNV areas were compared among each group. The experiments were repeated three times, with similar results. Data are mean ± SE. $*p < 0.01$. (**D**) *vegf* mRNA levels were compared in laser-treated WT and IL-17 KO mice at several time points ($n = 3$). The experiments were repeated three times, with similar results. Data are mean ± SE. $*p < 0.05$. (**E**) WT mice were inoculated with control IgG (10 ng/μl; 2 μl), anti–IL-17 Ab (2 μl, *left panel*), anti-VEGF Ab (2 μl, *right panel*) into the vitreous cavities immediately after laser treatment ($n = 10–15$). On day 7 after laser treatment, the sizes of CNV volumes were compared (*Figure legend continues*)

Ab (Fig. 1E, 1F). The combination of anti-VEGF and anti-IL-17 Abs was more effective than was the administration of either Ab alone (Fig. 1F). These data indicate that IL-17 has a strong potential for promoting neovascularization in a VEGF-independent manner in experimental CNV.

Although volume measurement by confocal microscopy was more sensitive than area measurement by conventional fluorescent microscopy, essentially similar effects were observed using these two methods (Fig. 1F). Thus, we primarily used area measurement in later experiments because of the convenience of fluorescence microscopy.

Infiltrated γδT cells and ILCs are the main source of IL-17 in the laser-treated eye

IL-17 was shown to be secreted not only from Th17 cells but also from innate immune cells (14), γδT cells (21), and invariant NKT (iNKT) cells (22). Based on these reports, we performed intracellular staining to investigate which cells produce IL-17 in the laser-treated eye. The number of IL-17$^+$ cells increased after laser treatment (Fig. 2A, *upper panels*). Approximately 70% of IL-17$^+$ cells were also CD3$^+$, and most of these IL-17$^+$ cells were γδT cells not Th17 cells (Fig. 2A, *lower panels*). The other 30% of the IL-17$^+$ cells were CD45$^+$ but CD3$^-$ and also Thy-1$^+$ and Lin$^-$ (CD11b, B220, NK1.1, Gr-1), suggesting that ~30% of IL-17–producing cells in choroid regions exhibiting CNV are ILCs (Fig. 2B). These cells were negative for NKp46, CD127, CD122, and CD25, suggesting that these ILCs were not LTi or ILC22 (data not shown). In this fraction, both Sca1$^+$ and Sca1$^-$ cells were included, suggesting a mixture of heterogeneous populations.

Immunohistochemical analysis of retina and RPE/choroid sections revealed that γδT cells infiltrated into laser-injury lesions in the choroid regions (Fig. 2C). Furthermore, IL-17–producing γδT cells were completely absent in the laser-treated eyes of mice lacking RORγt, a master transcription factor for IL-17 transcription (23, 24) (Fig. 2D). These results indicate that infiltrating γδT cells are the main source of IL-17 in the eye after laser treatment. To clarify the importance of infiltrating γδT cells in CNV development, we examined TCRγδ KO mice and found that their *Il17a* mRNA expression levels, as well as their IL-17$^+$ cell counts, were significantly lower than those in WT mice (Fig. 2E, 2F). The areas of CNV after laser treatment were smaller in TCRγδ KO mice than in WT mice (Fig. 2G). Although not statistically significant, administration of Ab against IL-17 always decreased the size of CNV areas in TCRγδ KO mice or Rag2-deficient mice, suggesting a small contribution of IL-17–producing ILCs to CNV formation (Fig. 2G, data not shown for Rag2$^{-/-}$ mice). Adoptive transfer of T lymphocytes into Rag2-deficient (*rag2*KO) mice confirmed that γδT cells, but not conventional CD4$^+$ T cells, were the major producers of IL-17 and that they greatly contributed to ocular neovascularization after laser injury (Fig. 2H). These data suggest that IL-17, as well as IL-17–producing cells, could be therapeutic targets in the treatment of CNV. In addition, targeting the mechanism of IL-17 production in the injured eye could be a useful means of preventing CNV.

IL-1β, but not IL-23, plays a pivotal role in IL-17 induction and laser-induced CNV

Next, we investigated which innate cytokines induce IL-17 from γδT cells, because targeting the mechanism of IL-17 production in the injured eye could be a useful means of preventing CNV. IL-23 was reported to be indispensable in the proliferation of these cells and in their ability to produce IL-17 (25, 26). However, to our surprise, the degree to which CNV areas developed in IL-23p19 KO mice was identical to or only slightly less than that seen in WT mice (Fig. 3A). IL-17$^+$ γδT cells, as well as *Il17a* mRNA, were present in the IL-23p19 KO mice, although IL-17 levels were slightly lower in these mice than in WT mice (Fig. 3B, 3C). These results suggest that IL-23 plays a limited role in IL-17 induction, and there is an IL-23–independent mechanism that stimulates IL-17 production from γδT cells.

Because IL-1β was shown to play a crucial role in inducing IL-17 production in vivo (26), we investigated its role next. IL-1β was shown to be rapidly upregulated in laser-induced CNV (8). We noticed that *Il1b* mRNA levels in the CNV regions were higher in IL-23p19 KO mice than in WT mice (data not shown), suggesting that IL-1β may be more important than IL-23 in the laser-induced CNV model. To test this, we blocked the effect of IL-1β using an IL-1R antagonist (IL-1ra). Consistent with the results of a previous report (8), treatment of mice with IL-1ra reduced the size of the CNV areas in both WT and IL-23p19 KO mice (Fig. 4A). IL-1ra treatment also reduced *Il17a* mRNA levels and the number of IL-17–producing cells in both WT and IL-23p19 KO mice (Fig. 4B, 4C). The number of IL-17–producing cells was not significantly different between WT and IL-23 KO mice, although we always observed some reduction of IL-17$^+$ cells in IL-23 KO mice. Furthermore, IL-1β potently induced IL-17 production from γδT cells more efficiently than did IL-23 in vitro (Fig. 4D). These data indicate that IL-1β, rather than IL-23, plays more important roles in the induction of IL-17–producing γδT cells, as well as laser-induced CNV formation in the eye.

HMGB-1 as an inducer of IL-1β from macrophages and IL-17 from γδT cells

Given that IL-1β was shown to be mostly produced from macrophages (27), we investigated the endogenous TLR ligand that can induce macrophages to produce IL-1β. We confirmed that CNV areas were smaller in TLR2- and TLR4-deficient mice than in WT mice (Fig. 5A). HMGB-1 was reported to be involved in Th17 development in an experimental autoimmune encephalomyelitis model (28) and to play important roles in alkaline-induced corneal neovascularization through TLR4 (29). We observed that HMGB-1 also upregulated IL-17 secretion from γδT cells in collaboration with IL-1β (Fig. 4D). Thus, we investigated the role of HMGB-1 in IL-17 induction in our laser-induced CNV model. HMGB-1 proteins are usually contained in the nucleus but can be released into the extracellular milieu as the result of injury or other forms of stress (30). In the retina, degenerated photoreceptors exhibit augmented HMGB-1 expression after retinal detachment (31). HMGB-1 mRNA expression was increased soon after laser exposure (Fig. 5B). HMGB-1 ex-

among the four groups. The experiments were repeated three times, with similar results. Data are mean ± SE. *$p < 0.01$. (**F**) WT mice were inoculated with control IgG (10 ng/μl, 2 μl), anti–IL-17 Ab (10 ng/μl; 2 μl), anti-VEGF Ab (10 ng/μl; 2 μl), or the combination of anti–IL-17 (20 ng/μl; 1 μl) and anti-VEGF Abs (20 ng/μl; 1 μl) into the vitreous cavities immediately after laser treatment (n = 10–15). Representative CNV lesions of choroidal flat mounts of each group are shown on day 7 after laser treatment. Arrowheads indicate stained CNV tissues. Scale bars, 100 μm. The sizes of CNV volumes and areas were compared among four groups. The experiments were repeated three times, with similar results. Data are mean ± SE. *$p < 0.01$.

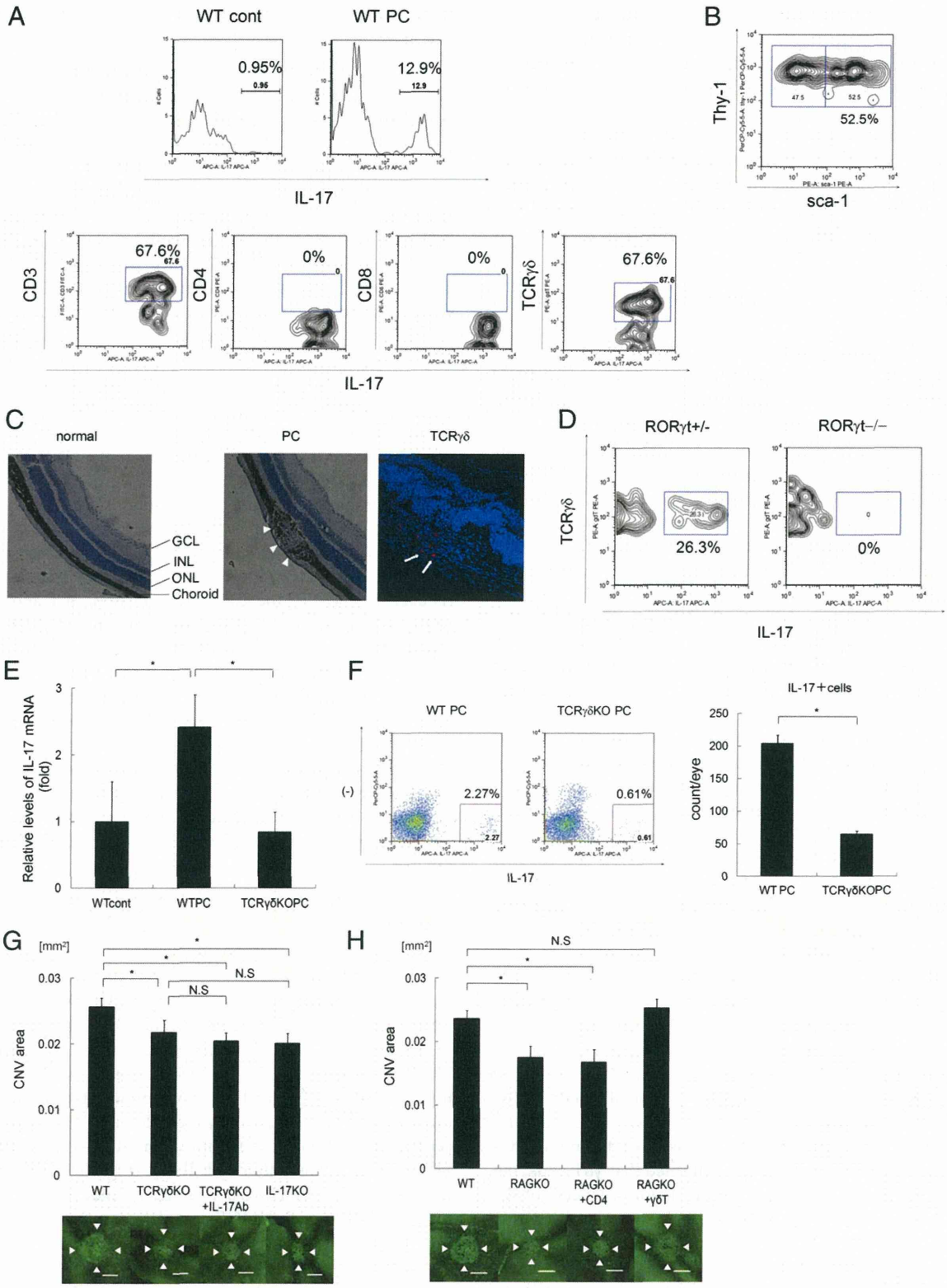

FIGURE 2. The source of IL-17 in the laser-treated eye. (**A**) Ocular-infiltrating cells were analyzed 4 d after laser treatment. The production of IL-17A in cells was examined by intracellular staining. WT laser-treated eye samples gated for $CD45^+$ cells (*upper panels*). Samples gated for IL-$17A^+$ cells (*lower panels*). One representative experiment of three independent experiments is shown. (**B**) The IL-$17A^+$ cell population in TCRγδ KO mice was analyzed for Thy-1 and Sca-1 expression levels by flow cytometry. (**C**) Immunohistochemical analysis of retina and RPE/choroid sections on day 4 after laser treatment. H&E staining of the retina and RPE/choroid sections of control and laser-treated mice (*left* and *middle panel*, respectively). The retina and RPE/choroid sections were stained with anti-TCRγδ (red) (arrow in *right panel*). Representative images are shown. Arrowheads denote laser photocoagulated site. Original magnification ×10. (**D**) Intracellular staining data for IL-17A in laser-treated *Rorγt*$^{+/gfp}$ mice and *Rorγt*$^{gfp/gfp}$ mice on day 4 after laser treatment. The panels show the results of gating for TCRγδ$^+$ cells in laser-treated eye samples from each mouse. (**E**) Total RNA was extracted from the eyes of WT mice and TCRγδ KO mice on day 4 after laser treatment ($n = 3$). *Il17a* mRNA levels were normalized to *HPRT* levels in each sample. *$p < 0.01$. (**F**) Intracellular staining data on IL-17A in laser-treated WT mice and TCRγδ KO mice on day 4 after laser treatment ($n = 2$). The bar graph represents the fraction of the IL-$17A^+$ cell populations. The (*Figure legend continues*)

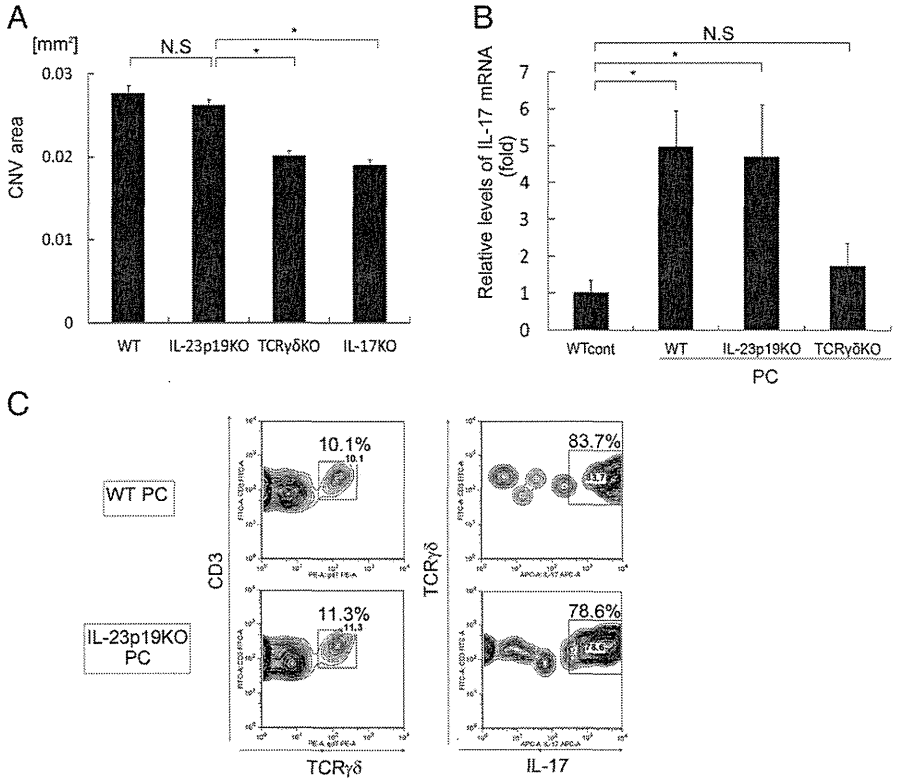

FIGURE 3. IL-17 induction and CNV promotion were independent of IL-23. (**A**) On day 4 after laser treatment, the sizes of CNV areas were compared among four groups: WT mice, IL-23p19 KO mice, TCRγδ KO mice, and IL-17 KO mice (n = 10–15). The experiment was repeated three times with similar results. Data are mean ± SE. *$p <$ 0.01. (**B**) The expression levels of *IL17a* mRNA in laser-treated eyes from WT mice, IL-23p19 KO mice, and TCRγδ KO mice were monitored using real-time PCR on day 4 after laser treatment, and the data were normalized to *HPRT* levels (n = 3). *$p <$ 0.01. (**C**) Ocular-infiltrating cells of WT mice (*upper panels*) and IL-23p19 KO mice (*lower panels*) were analyzed on day 4 after laser treatment (n = 2). Results of gating for CD3 (*left panels*) and TCRγδ$^+$ (*right panels*) cells are shown for each eye sample. The production of IL-17A in cells was examined by intracellular staining (*right panels*). One representative experiment of three independent experiments is shown.

pression was induced in RPE and photoreceptor cells at the laser-injured choroid (Fig. 5C). An Ab against HMGB-1 reduced the size of CNV areas (Fig. 5D), as well as the rate of infiltration of IL-17$^+$ γδT cells (Fig. 5E). HMGB-1 blockade reduced IL-1β production (Fig. 5F). Furthermore, rHMGB-1 induced IL-1β in a RAW macrophage cell line (Fig. 5G). Taken together, these findings indicate that injured photoreceptor cells express damage-associated molecular pattern molecules (DAMPs), including HMGB-1, which results in the induction of IL-1β, which, in turn, promotes IL-17 secretion from γδT cells. HMGB-1 may also directly stimulate IL-17 production from γδT cells in collaboration with IL-1β, because γδT cells were reported to respond to TLR ligands (32). As expected, rHMGB-1 upregulated IL-17 levels in γδT cells in vitro in the presence of IL-1β (Fig. 4D). Thus, reducing patients' levels of IL-1β or HMGB-1, similar to a reduction in IL-17 level, might be an effective strategy for the prevention of CNV (Fig. 6).

Discussion

The laser-induced CNV mouse model is well established for investigating ocular angiogenesis (33). As with human AMD, suppression of angiogenesis by an anti-VEGF Ab is therapeutic for laser-induced CNV (18). This model system is eminently useful for identifying promising therapeutic targets for human AMD. For example, Takeda et al. (34) identified CCR3, a receptor found on eosinophils and mast cells, which are immune mediators of allergic inflammation, as an essential chemokine receptor for the growth of choroidal vessels in CNV. They demonstrated that blockade of intraocular CCR3 with neutralizing Abs or receptor antagonists significantly decreased the generation of abnormal blood vessels in the choroid after laser injury in a CNV mouse model. CCR3 was shown to be expressed in the endothelial cells lining the abnormal blood vessels of CNV in wet AMD patients, suggesting that the eotaxin–CCR3 axis is functional in human disease.

In the current study, we demonstrated that IL-17 plays an important role in promoting ocular neovascularization, and γδT cells, as well as a small fraction of ILCs, are the main sources of IL-17 in this laser-injury model. A recent study showed that IL-17 and IL-22 are elevated in the sera of AMD patients and that C5a promotes the production of these cytokines from human CD4$^+$ T cells (15). In our experimental CNV mouse model, γδT cells, rather than Th17 cells, were the major (~70%) source of IL-17. Another recent study showed that γδT cells express a C5a receptor and promote IL-17 production by C5a stimulation (35). However, because laser-induced CNV is an acute-injury model, the role of C5a in this system remains to be clarified.

Interestingly, VEGF levels were not affected by IL-17 deficiency (Fig. 1D). This suggests that IL-17 functions as a proangiogenic factor in a VEGF-independent manner, and anti–IL-17 therapy could be useful for patients resistant to anti-VEGF therapy. Moreover, a combined therapy aimed at these two

experiments were repeated three times with similar results. Data are mean ± SE. *$p < 0.01$. (**G**) On day 7 after laser treatment, the sizes of CNV areas were evaluated and compared among WT mice, IL-17 KO mice, TCRγδ KO mice, and TCRγδ KO mice with Ab to IL-17 (10 ng/μl; 2 μl) inoculation into the vitreous cavities immediately after laser treatment (n = 10–15). Data are mean ± SE. The experiment was repeated three times with similar results. Arrowheads indicate stained CNV tissues. Scale bars, 100μm. *$p < 0.01$. (**H**) A total of 3×10^5 CD3$^+$CD4$^-$TCRγδ$^+$ cells from WT mice or 1×10^6 CD3$^+$CD4$^+$TCRγδ$^-$ cells from WT mice, purified by means of flow cytometry, were injected i.v. into *Rag2* KO mice. At 4 d after cell transfer, the mice were subjected to laser treatment. On day 7 after laser treatment, eyes were enucleated for evaluation of CNV. Arrowheads indicate stained CNV tissues. Scale bars, 100μm. *$p < 0.01$. GCL, Ganglion cell layer; INL, inner nuclear layer; ONL, outer nuclear layer.

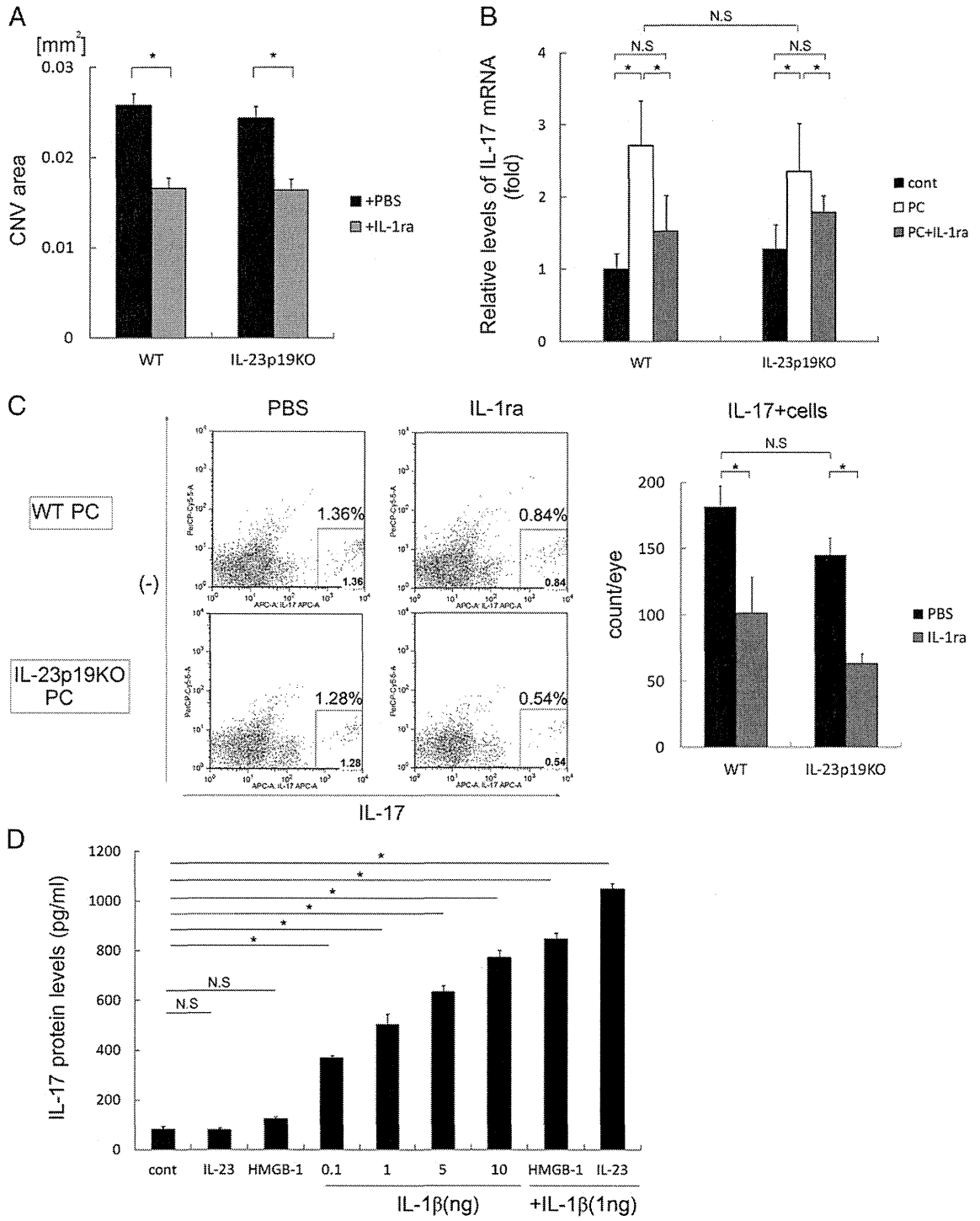

FIGURE 4. Suppression of IL-17 induction and CNV by blockade of IL-1β. (**A–C**) WT mice and IL-23p19 KO mice were subjected to laser treatment and inoculated with IL-1ra (1 ng/μl; 2 μl) or PBS (2 μl) into the vitreous cavities immediately after laser treatment. (A) The sizes of CNV areas were compared in WT mice and IL-23p19 KO mice inoculated with IL-1ra or PBS on day 7 (n = 10–15). (B) The expression levels of *Il17a* mRNA in laser-treated eyes from WT mice and IL-23p19 KO mice were monitored on day 4 by real-time PCR, and the data were normalized to HPRT expression (n = 3). Data are mean ± SE. *$p < 0.01$. (C) Intracellular staining data for IL-17A in laser-treated WT and IL-23p19 KO mice on day 4 after laser treatment (n = 2). The bar graph represents the fraction of the IL-17A$^+$ cell populations. The experiments were repeated three times with similar results. Data are mean ± SE. *$p < 0.01$. (**D**) A total of 1×10^5 γδT purified cells from WT mice was cultured with anti-CD3 in the presence of IL-1β, with or without IL-23 and HMGB-1. After 48 h, the amount of secreted IL-17 protein in the supernatants was measured using ELISA. Data are mean ± SE. *$p < 0.01$.

cytokines may be more powerful than a single-treatment approach. Although there are a number of reports suggesting that IL-17 promotes angiogenesis by directly stimulating endothelial cells, the precise mechanism of angiogenesis by IL-17 is not clear. Other reports indicate that VEGF is induced by IL-17 (11). Thus, we could not completely rule out the possibility that VEGF induced by IL-17 participates in CNV formation in WT animals (Fig. 6).

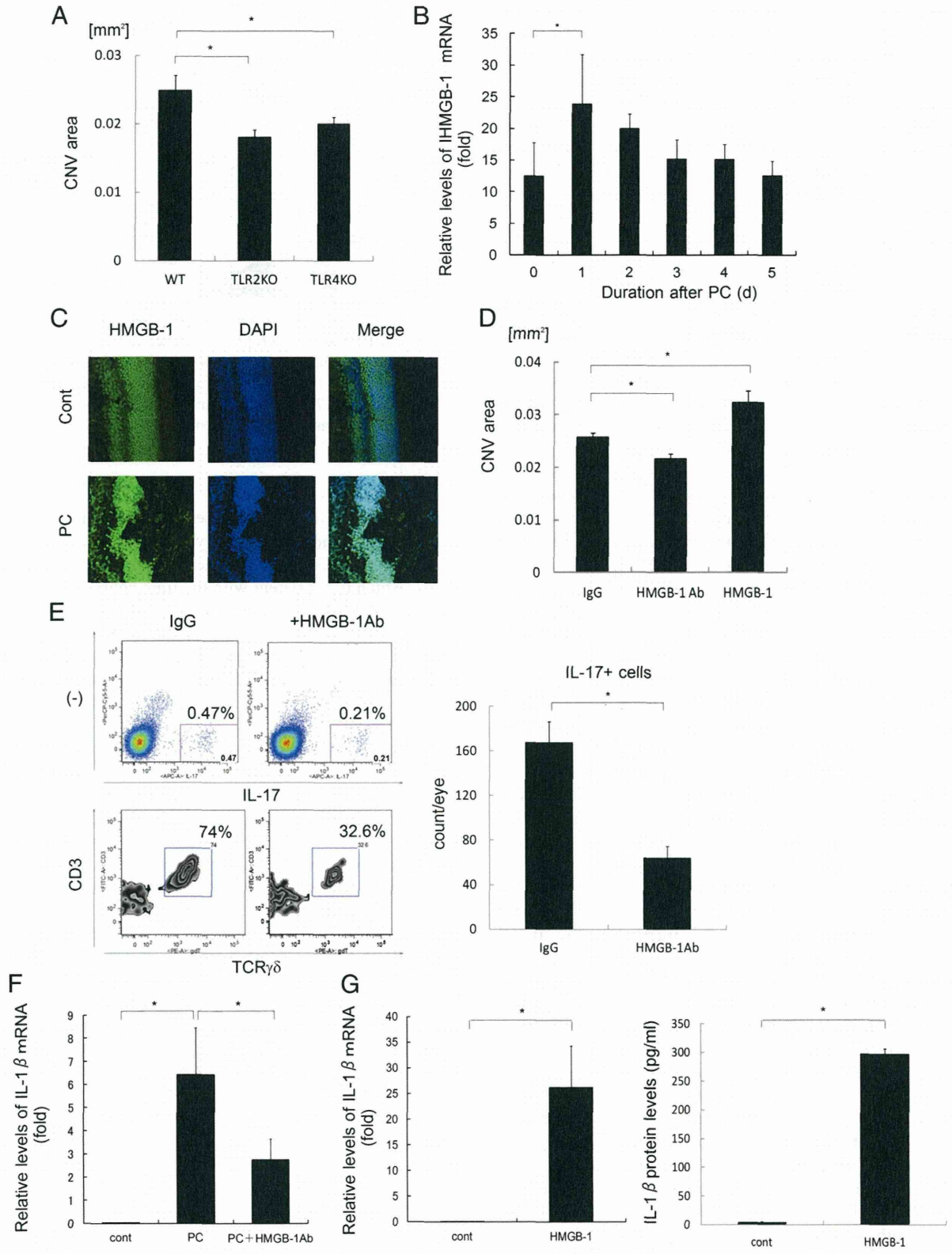

FIGURE 5. Suppression of IL-17 and IL-1β induction by blockade of HMGB-1. (**A**) On day 7 after laser treatment, the sizes of CNV areas were compared among WT, TLR2, and TLR4 KO mice (n = 10–12). The experiments were repeated three times with similar results. Data are mean ± SE. *$p < 0.01$. (**B**) Total RNA was extracted from the eyes of WT mice on the indicated days after laser treatment (n = 3). *HMGB-1* mRNA levels were normalized to HPRT levels in each sample. Data are mean ± SE. *$p < 0.05$. (**C**) Immunohistochemical analysis of normal retina and RPE/choroid sections (*upper panels*) or retina and RPE/choroid sections 4 d after laser treatment (*lower panels*). The retina and RPE/choroid sections were double stained with anti–HMGB-1 (green) and DAPI (blue). Original magnification ×10. (**D**) On day 7 after laser treatment, the sizes of the CNV areas were compared among WT mice inoculated with control IgG, Ab to HMGB-1, or HMGB-1 into the vitreous cavities immediately after laser treatment (n = 10–15). Data are mean ± SE. *$p < 0.01$. (**E**) Intracellular staining data for IL-17A in laser-treated WT mice on day 4 with or without Ab to HMGB-1 inoculation into the vitreous cavities immediately after laser treatment (n = 2) (*upper panels*). Results of gating for IL-17A$^+$ cells (*lower panels*). The bar graph represents the fraction of the IL-17A$^+$ cell populations. The experiments were repeated (*Figure legend continues*)

In addition to γδT cells, we found that 30% of IL-17 came from $CD3^-Thy1^+$ ILCs. In this fraction, both $Sca1^+$ and $Sca1^-$ cells were included; therefore, a mixture of heterogeneous populations is likely. However, IL-17 production was completely dependent on RORγt. Because IL-17–producing ILCs are reported as being mostly present in the gut (36), the origin of $IL\text{-}17^+$ ILCs in the eye is an intriguing subject. We showed that iNKT cells also play a role in CNV angiogenesis (6), but we could exclude the possibility that $IL\text{-}17^+$ ILCs were iNKT cells because those cells were $CD3^-$.

Another important feature of IL-17 production in the eye is the need for IL-23. IL-23 was reported to play critical roles in IL-17 production from conventional Th17 and γδT cells (26). For example, IL-17 production from Th17 cells and γδT cells infiltrated into the brain was completely dependent on IL-23 in an experimental autoimmune encephalomyelitis model and a brain ischemia model, respectively (17, 21). IL-23 was shown to be a potent inducer of inflammation in autoimmune diseases, RA, psoriasis, encephalomyelitis, and inflammatory bowel diseases. However, in our current study, we demonstrated that γδT cells can produce IL-17 without IL-23 (Fig. 3). With regard to Th17 cells, TGF-β plus IL-6 was shown to be necessary for early development of Th17 in vitro, and IL-23 is not necessary for early Th17 cell development in vitro, but it appears to be required for pathogenic features of Th17 cells. Izcue et al. (37) reported that TGF-β, rather than IL-23, was essential for Th17 development in vivo. However, it was shown that IL-23 is the most potent inducer of IL-17 from γδT cells. We examined other reported IL-17–inducing factors, including bacterial TLR ligands, as well as IL-6, and found that only IL-1β can act as a substitute for IL-23 in inducing IL-17 secretion from γδT cells (Fig. 4). In AMD patients, it was reported that accumulated macrophages in CNV areas and RPE cells secrete IL-1β (27). In mouse models, macrophages also infiltrate the eye (5), and IL-1β expression increases soon after laser treatment (8). Thus, we suspected that IL-1β is an essential factor in the induction of IL-17 from γδT cells, but we could not rule out other factors that stimulate TLRs. For example, we reported that *Chlamydia pneumonia* infection enhances CNV via TLR2 (38).

Because the laser CNV model is dependent on TLR2/4, we suspected that certain TLR ligands might stimulate IL-1β production from macrophages. However, no bacterial infection was evident in our laser-induced models; thus, endogenous DAMPs could be candidates. HMGB-1 protein, heat shock proteins, β-amyloid, and others were reported to be endogenous ligands for TLR and to function as DAMPs (39, 40). A recent study suggests that drusen components activate NLRP3, which induces IL-18, although drusen alone does not seem to activate TLRs (41). We investigated HMGB-1 because rHMGB-1, but not other recombinant proteins, including peroxiredoxins (42), potently induces IL-1β from macrophage-like cells. Secretion of IL-1β requires inflammasome activation, as well as TLR stimulation, and HMGB-1 seems to be able to activate both pathways simultaneously. The mechanism of inflammasome activation by HMGB-1 remains to be clarified. Our data indicated the possibility that HMGB-1 proteins play

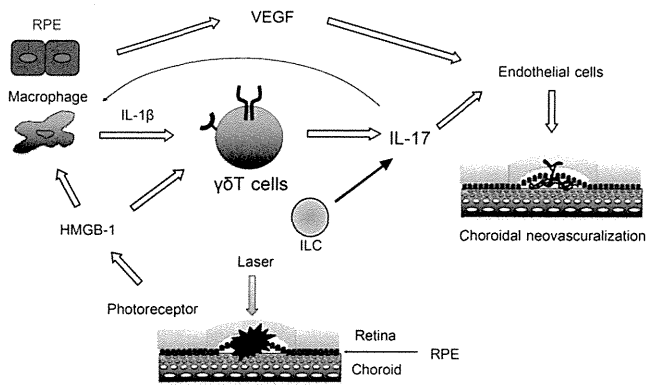

FIGURE 6. Schematic model for the promotion of CNV by IL-17, IL-1β, and HMGB-1. Macrophages are recruited into the injured choroid area and produce IL-1β in response to HMGB-1 stimulation. Then IL-1β induces IL-17 expression from infiltrated γδT cells. HMGB-1 also promotes IL-17 expression from γδT cells in combination with IL-1β. IL-17 functions as an angiogenic factor together with VEGF on endothelial cells.

specific roles at different phases after laser injury. HMGB-1 mRNA levels increased rapidly after laser injury (Fig. 5B). Thus, early HMGB-1 may induce IL-1β from macrophages on day 1, which is consistent with the time course of IL-1β mRNA expression. We also noticed maintained HMGB-1 protein expression in the laser-injured choroid on day 4 (Fig. 5C). We showed that HMGB-1 stimulated IL-17 production in combination with IL-1β from γδT cells. Thus, HMGB-1 protein may enhance IL-17 production from infiltrated γδT cells in a late phase after laser injury.

Apparently, IL-1β is proangiogenic, whereas Doyle et al. (41) showed that IL-18 is antiangiogenic, indicating that IL-1β and IL-18 have opposite functions in CNV formation. Doyle et al. (41) reported that LPS and the complement factor C1Q induced IL-1β at higher levels than IL-18 in vitro, and IL-1β mRNA expression was elevated from a few hours after laser stimulation in the laser-induced CNV model (8). We suspect that, in the early phase of injury, CNV is promoted by the NLRP3–IL-1β pathway, which is activated by strong DAMPs like HMGB-1, whereas, in a late phase, CNV is suppressed by the NLRP3–IL-18 pathway, which is activated by unknown DAMPs to promote tissue repair and remodeling or to maintain the choroidal homeostasis. Because little is known about the induction mechanisms of IL-1β and IL-18, the significance of these two related cytokines in CNV formation remains to be investigated.

The elevated IL-17 levels in the sera (15) suggest that increasing levels of IL-17 in the eye may be involved in the pathogenesis of AMD. Because humanized anti–IL-17 Ab is now in phase II trials for RA and psoriasis, anti–IL-17 therapy may become easily and rapidly applicable for AMD patients. We also expect that the suppression of innate cell activators, such as IL-1β and HMGB-1, could be preventive against the development of human AMD.

three times with similar results. Data are mean ± SE. $*p < 0.01$. (**F**) Total RNA was extracted from the eyes of WT mice, with or without Ab to HMGB-1 inoculation into the vitreous cavities immediately after laser treatment, on day 1 after laser treatment ($n = 3$). *Il1b* mRNA levels were normalized to *HPRT* levels in each sample. $*p < 0.01$. (**G**) RAW cells (2×10^5) were treated or not with 1 μM rHMGB-1 for 24 h. The expression levels of *Il1b* mRNA were monitored using real-time PCR, and the data were normalized to HPRT levels ($n = 3$). IL-1β protein levels in the culture supernatant were determined by ELISA. $*p < 0.01$.

Acknowledgments

We thank Dr. Y. Iwakura (Research Institute for Biomedical Sciences, Tokyo University of Science, Chiba, Japan) for IL-17 KO mice, Dr. D. Cua (Schering-Plough Biopharma, DNAX Discovery Research, Palo Alto, CA) for IL-23 KO mice, and Dr. S. Akira (Laboratory of Host Defense, Osaka University) for TLR2/4 KO mice.

Disclosures

The authors have no financial conflicts of interest.

References

1. Lim, L. S., P. Mitchell, J. M. Seddon, F. G. Holz, and T. Y. Wong. 2012. Age-related macular degeneration. *Lancet* 379: 1728–1738.
2. Tuo, J., S. Grob, K. Zhang, and C. C. Chan. 2012. Genetics of immunological and inflammatory components in age-related macular degeneration. *Ocul. Immunol. Inflamm.* 20: 27–36.
3. Telander, D. G. 2011. Inflammation and age-related macular degeneration (AMD). *Semin. Ophthalmol.* 26: 192–197.
4. Grossniklaus, H. E., J. X. Ling, T. M. Wallace, S. Dithmar, D. H. Lawson, C. Cohen, V. M. Elner, S. G. Elner, and P. Sternberg, Jr. 2002. Macrophage and retinal pigment epithelium expression of angiogenic cytokines in choroidal neovascularization. *Mol. Vis.* 8: 119–126.
5. Tsutsumi, C., K. H. Sonoda, K. Egashira, H. Qiao, T. Hisatomi, S. Nakao, M. Ishibashi, I. F. Charo, T. Sakamoto, T. Murata, and T. Ishibashi. 2003. The critical role of ocular-infiltrating macrophages in the development of choroidal neovascularization. *J. Leukoc. Biol.* 74: 25–32.
6. Hijioka, K., K. H. Sonoda, C. Tsutsumi-Miyahara, T. Fujimoto, Y. Oshima, M. Taniguchi, and T. Ishibashi. 2008. Investigation of the role of CD1d-restricted invariant NKT cells in experimental choroidal neovascularization. *Biochem. Biophys. Res. Commun.* 374: 38–43.
7. Izumi-Nagai, K., N. Nagai, Y. Ozawa, M. Mihara, Y. Ohsugi, T. Kurihara, T. Koto, S. Satofuka, M. Inoue, K. Tsubota, et al. 2007. Interleukin-6 receptor-mediated activation of signal transducer and activator of transcription-3 (STAT3) promotes choroidal neovascularization. *Am. J. Pathol.* 170: 2149–2158.
8. Lavalette, S., W. Raoul, M. Houssier, S. Camelo, O. Levy, B. Calippe, L. Jonet, F. Behar-Cohen, S. Chemtob, X. Guillonneau, et al. 2011. Interleukin-1β inhibition prevents choroidal neovascularization and does not exacerbate photoreceptor degeneration. *Am. J. Pathol.* 178: 2416–2423.
9. Hasegawa, E., Y. Oshima, A. Takeda, K. Saeki, H. Yoshida, K. H. Sonoda, and T. Ishibashi. 2012. IL-27 inhibits pathophysiological intraocular neovascularization due to laser burn. *J. Leukoc. Biol.* 91: 267–273.
10. Moran, E. M., M. Connolly, W. Gao, J. McCormick, U. Fearon, and D. J. Veale. 2011. Interleukin-17A induction of angiogenesis, cell migration, and cytoskeletal rearrangement. *Arthritis Rheum.* 63: 3263–3273.
11. Ryu, S., J. H. Lee, and S. I. Kim. 2006. IL-17 increased the production of vascular endothelial growth factor in rheumatoid arthritis synoviocytes. *Clin. Rheumatol.* 25: 16–20.
12. Pickens, S. R., M. V. Volin, A. M. Mandelin, II, J. K. Kolls, R. M. Pope, and S. Shahrara. 2010. IL-17 contributes to angiogenesis in rheumatoid arthritis. *J. Immunol.* 184: 3233–3241.
13. Numasaki, M., J. Fukushi, M. Ono, S. K. Narula, P. J. Zavodny, T. Kudo, P. D. Robbins, H. Tahara, and M. T. Lotze. 2003. Interleukin-17 promotes angiogenesis and tumor growth. *Blood* 101: 2620–2627.
14. Cua, D. J., and C. M. Tato. 2010. Innate IL-17-producing cells: the sentinels of the immune system. *Nat. Rev. Immunol.* 10: 479–489.
15. Liu, B., L. Wei, C. Meyerle, J. Tuo, H. N. Sen, Z. Li, S. Chakrabarty, E. Agron, C. C. Chan, M. L. Klein, et al. 2011. Complement component C5a promotes expression of IL-22 and IL-17 from human T cells and its implication in age-related macular degeneration. *J. Transl. Med.* 9: 1–12.
16. Nakae, S., Y. Komiyama, A. Nambu, K. Sudo, M. Iwase, I. Homma, K. Sekikawa, M. Asano, and Y. Iwakura. 2002. Antigen-specific T cell sensitization is impaired in IL-17-deficient mice, causing suppression of allergic cellular and humoral responses. *Immunity* 17: 375–387.
17. Cua, D. J., J. Sherlock, Y. Chen, C. A. Murphy, B. Joyce, B. Seymour, L. Lucian, W. To, S. Kwan, T. Churakova, et al. 2003. Interleukin-23 rather than interleukin-12 is the critical cytokine for autoimmune inflammation of the brain. *Nature* 421: 744–748.
18. Krzystolik, M. G., M. A. Afshari, A. P. Adamis, J. Gaudreault, E. S. Gragoudas, N. A. Michaud, W. Li, E. Connolly, C. A. O'Neill, and J. W. Miller. 2002. Prevention of experimental choroidal neovascularization with intravitreal anti-vascular endothelial growth factor antibody fragment. *Arch. Ophthalmol.* 120: 338–346.
19. Oshima, Y., S. Oshima, H. Nambu, S. Kachi, K. Takahashi, N. Umeda, J. Shen, A. Dong, R. S. Apte, E. Duh, et al. 2005. Different effects of angiopoietin-2 in different vascular beds: new vessels are most sensitive. *FASEB J.* 19: 963–965.
20. Tanaka, K., K. Ichiyama, M. Hashimoto, H. Yoshida, T. Takimoto, G. Takaesu, T. Torisu, T. Hanada, H. Yasukawa, S. Fukuyama, et al. 2008. Loss of suppressor of cytokine signaling 1 in helper T cells leads to defective Th17 differentiation by enhancing antagonistic effects of IFN-gamma on STAT3 and Smads. *J. Immunol.* 180: 3746–3756.
21. Shichita, T., Y. Sugiyama, H. Ooboshi, H. Sugimori, R. Nakagawa, I. Takada, T. Iwaki, Y. Okada, M. Iida, D. J. Cua, et al. 2009. Pivotal role of cerebral interleukin-17-producing gammadeltaT cells in the delayed phase of ischemic brain injury. *Nat. Med.* 15: 946–950.
22. Michel, M. L., D. Mendes-da-Cruz, A. C. Keller, M. Lochner, E. Schneider, M. Dy, G. Eberl, and M. C. Leite-de-Moraes. 2008. Critical role of ROR-γt in a new thymic pathway leading to IL-17-producing invariant NKT cell differentiation. *Proc. Natl. Acad. Sci. USA* 105: 19845–19850.
23. Ivanov, I. I., B. S. McKenzie, L. Zhou, C. E. Tadokoro, A. Lepelley, J. J. Lafaille, D. J. Cua, and D. R. Littman. 2006. The orphan nuclear receptor RORgammat directs the differentiation program of proinflammatory IL-17+ T helper cells. *Cell* 126: 1121–1133.
24. Ichiyama, K., H. Yoshida, Y. Wakabayashi, T. Chinen, K. Saeki, M. Nakaya, G. Takaesu, S. Hori, A. Yoshimura, and T. Kobayashi. 2008. Foxp3 inhibits RORgammat-mediated IL-17A mRNA transcription through direct interaction with RORgammat. *J. Biol. Chem.* 283: 17003–17008.
25. Aggarwal, S., N. Ghilardi, M. H. Xie, F. J. de Sauvage, and A. L. Gurney. 2003. Interleukin-23 promotes a distinct CD4 T cell activation state characterized by the production of interleukin-17. *J. Biol. Chem.* 278: 1910–1914.
26. Sutton, C. E., S. J. Lalor, C. M. Sweeney, C. F. Brereton, E. C. Lavelle, and K. H. Mills. 2009. Interleukin-1 and IL-23 induce innate IL-17 production from gammadelta T cells, amplifying Th17 responses and autoimmunity. *Immunity* 31: 331–341.
27. Wang, J., K. Ohno-Matsui, T. Yoshida, N. Shimada, S. Ichinose, T. Sato, M. Mochizuki, and I. Morita. 2009. Amyloid-beta up-regulates complement factor B in retinal pigment epithelial cells through cytokines released from recruited macrophages/microglia: Another mechanism of complement activation in age-related macular degeneration. *J. Cell. Physiol.* 220: 119–128.
28. Su, Z., C. Sun, C. Zhou, Y. Liu, H. Zhu, S. Sandoghchian, D. Zheng, T. Peng, Y. Zhang, Z. Jiao, et al. 2011. HMGB1 blockade attenuates experimental autoimmune myocarditis and suppresses Th17-cell expansion. *Eur. J. Immunol.* 41: 3586–3595.
29. Lin, Q., X. P. Yang, D. Fang, X. Ren, H. Zhou, J. Fang, X. Liu, S. Zhou, F. Wen, X. Yao, et al. 2011. High-mobility group box-1 mediates toll-like receptor 4-dependent angiogenesis. *Arterioscler. Thromb. Vasc. Biol.* 31: 1024–1032.
30. Degryse, B., T. Bonaldi, P. Scaffidi, S. Müller, M. Resnati, F. Sanvito, G. Arrigoni, and M. E. Bianchi. 2001. The high mobility group (HMG) boxes of the nuclear protein HMG1 induce chemotaxis and cytoskeleton reorganization in rat smooth muscle cells. *J. Cell Biol.* 152: 1197–1206.
31. Arimura, N., Y. Ki-i, T. Hashiguchi, K. Kawahara, K. K. Biswas, M. Nakamura, Y. Sonoda, K. Yamakiri, A. Okubo, T. Sakamoto, and I. Maruyama. 2009. Intraocular expression and release of high-mobility group box 1 protein in retinal detachment. *Lab. Invest.* 89: 278–289.
32. Martin, B., K. Hirota, D. J. Cua, B. Stockinger, and M. Veldhoen. 2009. Interleukin-17-producing gammadelta T cells selectively expand in response to pathogen products and environmental signals. *Immunity* 31: 321–330.
33. Ryan, S. J. 1979. The development of an experimental model of subretinal neovascularization in disciform macular degeneration. *Trans. Am. Ophthalmol. Soc.* 77: 707–745.
34. Takeda, A., J. Z. Baffi, M. E. Kleinman, W. G. Cho, M. Nozaki, K. Yamada, H. Kaneko, R. J. Albuquerque, S. Dridi, K. Saito, et al. 2009. CCR3 is a target for age-related macular degeneration diagnosis and therapy. *Nature* 460: 225–230.
35. Han, G., S. Geng, Y. Li, G. Chen, R. Wang, X. Li, Y. Ma, B. Shen, and Y. Li. 2011. γδT-cell function in sepsis is modulated by C5a receptor signalling. *Immunology* 133: 340–349.
36. Buonocore, S., P. P. Ahern, H. H. Uhlig, I. I. Ivanov, D. R. Littman, K. J. Maloy, and F. Powrie. 2010. Innate lymphoid cells drive interleukin-23-dependent innate intestinal pathology. *Nature* 464: 1371–1375.
37. Izcue, A., S. Hue, S. Buonocore, C. V. Arancibia-Cárcamo, P. P. Ahern, Y. Iwakura, K. J. Maloy, and F. Powrie. 2008. Interleukin-23 restrains regulatory T cell activity to drive T cell-dependent colitis. *Immunity* 28: 559–570.
38. Fujimoto, T., K. H. Sonoda, K. Hijioka, K. Sato, A. Takeda, E. Hasegawa, Y. Oshima, and T. Ishibashi. 2010. Choroidal neovascularization enhanced by *Chlamydia pneumoniae* via Toll-like receptor 2 in the retinal pigment epithelium. *Invest. Ophthalmol. Vis. Sci.* 51: 4694–4702.
39. Yanai, H., T. Ban, Z. Wang, M. K. Choi, T. Kawamura, H. Negishi, M. Nakasato, Y. Lu, S. Hangai, R. Koshiba, et al. 2009. HMGB proteins function as universal sentinels for nucleic-acid-mediated innate immune responses. *Nature* 462: 99–103.
40. Zhang, Q., M. Raoof, Y. Chen, Y. Sumi, T. Sursal, W. Junger, K. Brohi, K. Itagaki, and C. J. Hauser. 2010. Circulating mitochondrial DAMPs cause inflammatory responses to injury. *Nature* 464: 104–107.
41. Doyle, S. L., M. Campbell, E. Ozaki, R. G. Salomon, A. Mori, P. F. Kenna, G. J. Farrar, A. S. Kiang, M. M. Humphries, E. C. Lavelle, et al. 2012. NLRP3 has a protective role in age-related macular degeneration through the induction of IL-18 by drusen components. *Nat. Med.* 18: 791–798.
42. Shichita, T., E. Hasegawa, A. Kimura, R. Morita, R. Sakaguchi, I. Takada, T. Sekiya, H. Ooboshi, T. Kitazono, T. Yanagawa, et al. 2012. Peroxiredoxin family proteins are key initiators of post-ischemic inflammation in the brain. *Nat. Med.* 18: 911–917.

PLOS ONE

A Novel Platelet-Activating Factor Receptor Antagonist Inhibits Choroidal Neovascularization and Subretinal Fibrosis

Han Zhang[1,2]*, Yang Yang[1], Atsunobu Takeda[1], Takeru Yoshimura[1], Yuji Oshima[1], Koh-Hei Sonoda[3], Tatsuro Ishibashi[1]

1 Department of Ophthalmology, Graduate School of Medical Sciences, Kyushu University, Fukuoka, Japan, **2** Department of Ophthalmology, the First Hospital of China Medical University, Shenyang, China, **3** Department of Ophthalmology, Yamaguchi University Graduate School of Medicine, Ube, Yamaguchi, Japan

Abstract

Choroidal neovascularization (CNV) is a critical pathogenesis in age-related macular degeneration (AMD), the most common cause of blindness in developed countries. To date, the precise molecular and cellular mechanisms underlying CNV have not been elucidated. Platelet-activating factor (PAF) has been previously implicated in angiogenesis; however, the roles of PAF and its receptor (PAF-R) in CNV have not been addressed. The present study reveals several important findings concerning the relationship of the PAF-R signaling with CNV. PAF-R was detected in a mouse model of laser-induced CNV and was upregulated during CNV development. Experimental CNV was suppressed by administering WEB2086, a novel PAF-R antagonist. WEB2086-dependent suppression of CNV occurred via the inhibition of macrophage infiltration and the expression of proangiogenic (vascular endothelial growth factor) and proinflammatory molecules (monocyte chemotactic protein-1 and IL-6) in the retinal pigment epithelium–choroid complex. Additionally, WEB2086-induced PAF-R blockage suppresses experimentally induced subretinal fibrosis, which resembles the fibrotic subretinal scarring observed in neovascular AMD. As optimal treatment modalities for neovascular AMD would target the multiple mechanisms of AMD-associated vision loss, including neovascularization, inflammation and fibrosis, our results suggest PAF-R as an attractive molecular target in the treatment of AMD.

Citation: Zhang H, Yang Y, Takeda A, Yoshimura T, Oshima Y, et al. (2013) A Novel Platelet-Activating Factor Receptor Antagonist Inhibits Choroidal Neovascularization and Subretinal Fibrosis. PLoS ONE 8(6): e68173. doi:10.1371/journal.pone.0068173

Editor: Christoph Englert, Leibniz Institute for Age Research - Fritz Lipmann Institute (FLI), Germany

Received November 4, 2012; **Accepted** May 28, 2013; **Published** June 27, 2013

Funding: This work was supported by grants C (K-H.S.) and grant-in-aid for Young Scientists (A) (A.T.) from the Ministry of Education, Science, Sports and Culture of Japan. The funders had no role in study design, data collection and analysis, decision to publish, or preparation of the manuscript.

Competing Interests: The authors have declared that no competing interests exist.

* E-mail: zhanghan0614@139.com

Introduction

Neovascular age-related macular degeneration (AMD) leads to severe deterioration of central vision in elderly individuals owing to the development of choroidal neovascularization (CNV) in the macular region [1]. Abnormal new blood vessels initially proliferate under Bruch's membrane and the retinal pigment epithelium (RPE) and then invade the subretinal space, leading to subretinal hemorrhages, exudative lesions, serous retinal detachment, and ultimately disciform scarring [2]. Local destruction of photoreceptors, RPE, and choroidal blood vessels leads to irreversible loss of macular function and vision.

CNV is regarded as a submacular wound healing process that requires a continually evolving interaction among cells, cytokines, and the extracellular matrix [2,3]. Angiogenesis is an essential component of this process, and current clinical strategies for treating CNV are primarily aimed at inhibiting vascular endothelial growth factor (VEGF), the major promoter of angiogenesis [4,5]. However, overall only 30%–40% of exudative AMD patients gain three lines in visual acuity, and approximately 1 in 6 patients experience progressive loss in visual acuity that leads to legal blindness despite standard treatment with potent VEGF inhibitors [6–8]. These results are not surprising because angiogenesis is only one component of the wound healing process and because CNV pathogenesis extends beyond the endothelium. Therefore, CNV may be amenable to additional therapeutic alternatives besides anti-angiogenesis. During the past decade, several studies have examined the immune mechanisms in AMD and have reached the consensus that inflammation is a key driver in the development of neovascular AMD [2,3,9–11]. AMD is regarded as the result of an ongoing low-grade chronic inflammatory process, much like Alzheimer's disease and other chronic diseases of aging. This inflammatory process includes macrophage infiltration and the regulation of cytokine networks, which mediate CNV development [9].

Platelet-activating factor (PAF, 1-O-alkyl-2-acetyl-sn-glycero-3-phosphocholine), the first bioactive lipid ever identified, is a potent proinflammatory mediator that is involved in cellular activation, intracellular signaling, apoptosis, and diverse inflammatory reactions [12–15]. Its biological actions are mediated through the activation of a G protein-coupled PAF receptor (PAF-R) [16]. Several studies have suggested the involvement of PAF in angiogenesis. PAF directly stimulates the *in vitro* migration of endothelial cells, enhances vascular permeability, and promotes *in vivo* angiogenesis [17–21]. The results of animal studies suggest that PAF may contribute to the angiogenic activity of certain

cytokines by stimulating the production of VEGF, tumor necrosis factor-alpha, and hepatocyte growth factor [19,22,23]. A recent study shows that PAF-R is present in RPE cells and choroidal endothelial cells, and PAF upregulates VEGF in RPE cells [24]. Because these cell types are important for CNV development, these findings suggest that PAF may be involved in the pathogenesis of neovascular AMD. However, *in vivo* evidence supporting the role of PAF and PAF-R in CNV has not been reported.

In the present study, we demonstrate that local expression of PAF-R in the subretinal space is upregulated during CNV development. Administration of the PAF-R antagonist potently attenuated CNV lesion size by suppressing macrophage infiltration and the expression of multiple CNV-related molecules in the injured eye. We further report that PAF-R blockage inhibits experimental subretinal fibrosis. Thus, PAF-R blockage may provide a novel, effective treatment for neovascular AMD.

Materials and Methods

Animals

Female 7- to 10-week-old C57BL/6 mice were purchased from Japan SLC (Shizuoka, Japan) and used in all experiments. All animal experiments were approved by the Committee on the Ethics of Animal Experiments, Graduate School of Medical Sciences, Kyushu University, Japan. Animals were treated according to the ARVO Statement for the Use of Animals in Ophthalmic and Vision Research.

Induction and Evaluation of CNV

CNV was induced by photocoagulation as described previously, with some modifications [25]. In brief, laser photocoagulation was applied around the optic disc using a 532-nm diode laser (200 mW, 0.1-s duration, 75-μm diameter; Iridex, Mountain View, CA) to burn the posterior pole of the retina (4 spots/eye). Only lesions in which a subretinal bubble developed were used in subsequent experiments. Ten days after photocoagulation, the mice were anesthetized and perfused with 50 mg/ml of fluorescein-labeled dextran (2×10^6 average molecular weight; Sigma, St. Louis, MO). Following enucleation and fixation in 4% paraformaldehyde, corneas and lenses were removed, and each entire retina was dissected from the eye cup. After each eye cup was flat-mounted, the total area of hyperfluorescence associated with each burn was measured using ImageJ software (National Institutes of Health, Bethesda, MD).

Treatment with PAF-R Antagonist

Animals were treated with the PAF-R antagonist WEB2086 (Santa Cruz Biotechnology, Santa Cruz, CA) or phosphate-buffered saline (PBS, used as vehicle) 1 h before photocoagulation, and treatments were continued daily until the end of the study. WEB2086 was administered intraperitoneally to mice at 5 mg/kg body weight.

In some experiments, mice were injected intravitreally with 1 μg WEB2086 in 0.5 μl of PBS immediately after laser photocoagulation using 32-gauge needles (Hamilton, Reno, NV) under an operating microscope. Injections were repeated every other day for the duration of the study.

Immunohistochemistry and Immunofluorescence

For PAF-R staining, cryostat sections (6-μm thick) from naïve and laser-treated eyes (5 days after photocoagulation) were incubated with polyclonal rabbit anti-PAF-R antibody (1:400, Santa Cruz Biotechnology) and bovine anti-rabbit IgG-HRP (Santa Cruz Biotechnology), followed by the chromogen AEC (Vector Laboratories, Burlingame, CA). To bleach the pigment in RPE and choroid, the sections were incubated in 3% H_2O_2 for 18 h at room temperature and then counterstained in hematoxylin.

The FITC-conjugated endothelial cell marker isolectin B4 (1:200, Vector Laboratories) and the R-PE-conjugated rat anti-mouse macrophage marker F4/80 (1:100, Invitrogen, Carlsbad, CA) were used for double immunofluorescence staining of choroidal flat mounts (3 days after photocoagulation). The area of F4/80-positive cells within and near the laser lesions was measured using ImageJ and normalized to the size of CNV (100%).

Quantitative Real-time Reverse Transcription Polymerase Chain Reaction (qRT-PCR)

Total RNA was extracted using TRIzol reagent (Invitrogen) from RPE–choroid complexes at various times after CNV induction. Aliquots containing 1 μg of total RNA were reverse transcribed using a first-strand cDNA synthesis kit (Roche Diagnostics GmbH, Mannheim, Germany) according to the manufacturer's instructions. qRT-PCR was performed using LightCycler (Roche Diagnostics GmbH) and SYBR green real-time PCR mix (Takara Bio, Otsu, Shiga, Japan). Target sequences were amplified using the following primer pairs: PAF-R, 5′-TTGCCTGAGCCATCCTTATT-3′ and 5′-CCTCCCACTGTGGATTGTCT-3′; VEGF, 5′-GTTCACTGTGAGCCTTGTTCAG-3′ and 5′-GTCACATCTGCAAGTACGTTCG-3′; monocyte chemotactic protein (MCP)-1, 5′-AACTCTCACTGAAGCCAGCTCT-3′ and 5′-CGTTAACTGCATCTGGCTGA-3′; IL-6, 5′-TGGAGTCACAGAAGGAGTGGCTAAG-3′ and 5′-TCTGACCACAGTGAGGAATGTCCAC-3′; and β-actin, 5′-GATGACCCAGATCATGTTTGA-3′ and 5′-GGAGAGCATAGCCCTCGTAG-3′. All estimated mRNA levels were normalized to β-actin mRNA levels.

Enzyme-linked Immunosorbent Assay (ELISA)

RPE–choroid complexes were isolated at various time points following CNV induction and were immersed in 200 μl of tissue protein extraction reagent (T-PER; Pierce, Rockford, IL) supplemented with protease inhibitor cocktail (Halt; Pierce). The mixture was homogenized (Polytron; Kinematica AG) and clarified by centrifuging at 10,000 *g* for 5 min. VEGF, MCP-1, and IL-6 levels in the lysate were measured using the corresponding mouse VEGF, MCP-1, and IL-6 ELISA kit (R&D Systems, Minneapolis, MN) according to the manufacturer's protocols.

Induction and Evaluation of Subretinal Fibrosis

Recently, Jo et al. successfully established a mouse model of subretinal fibrosis, resembling the fibrotic subretinal scarring observed in advanced and late-stage neovascular AMD, by introducing inflammatory macrophages into the subretinal space [26]. This model is believed to prove a significant advance in investigating molecular mechanisms for neovascular AMD and establishing new therapy besides antiangiogenic approaches. In brief, C57BL/6 mice received an intraperitoneal injection of 2.5 ml of thioglycolate, and peritoneal exudate cells (PECs) were isolated after 3 days. PECs (4×10^7/ml) then were prepared for subretinal injection. Laser photocoagulation was performed in the posterior pole of each retina, and 0.5 μl of the prepared PECs was injected into each subretinal space using a blunt-tipped needle. Treated eyes that bled or did not exhibit focal retinal detachment

were excluded. WEB2086 (1 μg) or vehicle was injected intravitreally after 2 h, and injections were repeated every other day for the duration of the study. On day 7, the mice were euthanatized, and the PEC-injected eyes were removed. After dissecting the cornea and lens from each eye, radial relaxing incisions were made in the eye cups. Staining for glial fibrillary acidic protein (GFAP) was then performed to visualize the area of residual glia on choroidal flat mounts. The GFAP area was measured to quantify subretinal fibrosis because GFAP staining detects and quantitates subretinal fibrosis effectively in this animal model [26]. Polyclonal rabbit anti-GFAP antibody (1:400, Dako, Glostrup, Denmark) and FITC-conjugated anti-rabbit IgG (Invitrogen) were used for GFAP detection. Flat mounts were observed using a fluorescence microscope, and GFAP areas were measured using ImageJ.

Statistical Analysis

Each result is representative of at least three independent experiments. All values represent mean ± SD. Statistical significance was assessed using Student's t-test (SPSS, Chicago, IL). $P<0.05$ was considered statistically significant.

Results

PAF-R Expression during Laser-induced CNV Development

PAF-R expression during the development of laser-induced CNV was measured by qRT-PCR (Figure 1A). PAF-R mRNA level was elevated significantly ($P<0.01$) on day 3 after photocoagulation. By day 5, PAF-R mRNA peaked at levels 6.5-fold higher than the levels at the 0-h baseline ($P<0.01$). PAF-R expression decreased on day 7, but it remained elevated above the baseline on day 10 ($P<0.05$). Immunohistochemical staining confirmed the presence of PAF-R in RPE cells and choroidal endothelial cells of naïve samples (Figure 1B), and PAF-R signals became stronger in CNV regions on day 5 after photocoagulation (Figure 1C). Under high magnification, RPE-like cells and endothelial cells in CNV showed PAF-R positivity (data not shown).

Suppression of CNV with WEB2086-induced PAF-R Blockage

CNV areas on flat mounts were measured to evaluate the effects of WEB2086, a PAF-R antagonist, on CNV development. The typical features of experimental CNV in PBS-treated mice 10 days after photocoagulation included broad, flat neovascular nets (Figure 2A and 2C). In contrast, only a few new vessels were observed in mice treated with both intraperitoneal (Figure 2B) and intravitreal (Figure 2D) injections of WEB2086. Quantitative measurement suggested that both systemic and local administration of WEB2086 significantly reduced the CNV area on day 10 ($P<0.001$ for both, Figure 2E). The neovascular response in mice treated intravitreally was suppressed to a slightly greater, but non-significant, extent compared with that in mice treated intraperitoneally. Histological examination indicated no signs of retinal toxicity for intravitreal administration of WEB2086 at this dose (data not shown).

Reduction of Macrophage Infiltration in WEB2086-treated Eyes

We analyzed the infiltration of macrophages into CNV lesions on choroidal flat mounts by immunostaining for F4/80, a macrophage-specific marker. F4/80-positive cells were concentrated within the laser burns and around the edges of the laser scars 72 h after laser injury (Figure 3A). No F4/80-positive cells were observed outside the laser-burned area in the choroid. In comparison, WEB2086 treatment was associated with less infiltration of F4/80-positive cells (Figure 3B). Quantitative measurement of the F4/80-positive area indicated a 57% reduction in F4/80 positivity with WEB2086 treatment ($P<0.05$, Figure 3C). These data suggest that PAF-R blockage reduces inflammation in CNV lesions.

Inhibition of Proangiogenic and Proinflammatory Molecules with WEB2086

To elucidate the molecular mechanisms involved in the regulation of CNV by WEB2086-induced PAF-R blockage, we measured the mRNA levels of proangiogenic and proinflammatory mediators in RPE–choroid complexes during CNV development. The expression levels of VEGF and the proinflammatory mediators, MCP-1 and IL-6, were significantly elevated and peaked on days 1–3, respectively, following CNV induction in the PBS-treated mice (Figure 4A–C). In the WEB2086-treated mice, the expression levels of VEGF, MCP-1, and IL-6 were significantly reduced by 44%, 52%, and 43%, respectively, at the time of peak expression for each mediator ($P<0.01$ for all). Similarly, WEB2086-induced PAF-R blockage significantly suppressed the peak protein levels of VEGF, MCP-1, and IL-6 ($P<0.01$ for all), which were upregulated after CNV induction (Figure 4D–F). These results suggest that these mediators may be targets of the PAF-R signaling pathway during CNV development.

Suppression of Subretinal Fibrosis with WEB2086-induced PAF-R Blockage

Recently, we successfully established a mouse model of subretinal fibrosis that exhibits fibrotic subretinal scarring similar to that observed in advanced and late-stage neovascular AMD by introducing inflammatory macrophages into the subretinal space [26]. This model facilitates investigations of the molecular mechanisms of neovascular AMD and may assist in the establishment of novel therapies that go beyond antiangiogenic approaches. Using this animal model, we evaluated whether WEB2086-induced PAF-R blockage could mitigate subretinal fibrosis. Compared with the PBS-treated mice, the WEB2086-treated mice exhibited a reduced severity of subretinal fibrosis (Figure 5A and 5B). Quantitative measurement of the fibrosis area indicated that PAF-R blockage significantly reduced subretinal fibrosis by 66% ($P<0.001$, Figure 5C). These observations suggest that PAF-R signaling may be involved in the pathogenesis of subretinal fibrosis.

Discussion

To our knowledge, the present study is the first to characterize the relationship between PAF-R signaling and CNV. We observed PAF-R expression in laser-induced CNV and this expression increased during experimental CNV development. CNV was suppressed by blocking PAF-R using the novel receptor antagonist WEB2086. We report that the cellular and molecular mechanisms of WEB2086-induced CNV suppression included the inhibitory effects on macrophage infiltration and the expression of proangiogenic and proinflammatory molecules in the RPE–choroid complex. We also demonstrated that PAF-R blockage could suppress a model of experimental subretinal fibrosis that resembles the fibrotic subretinal scarring observed in neovascular AMD.

PAF-R has been cloned from several species and contains a seven-transmembrane domain typical of G protein-coupled receptors [16,27]. PAF-R mRNA has been identified in various

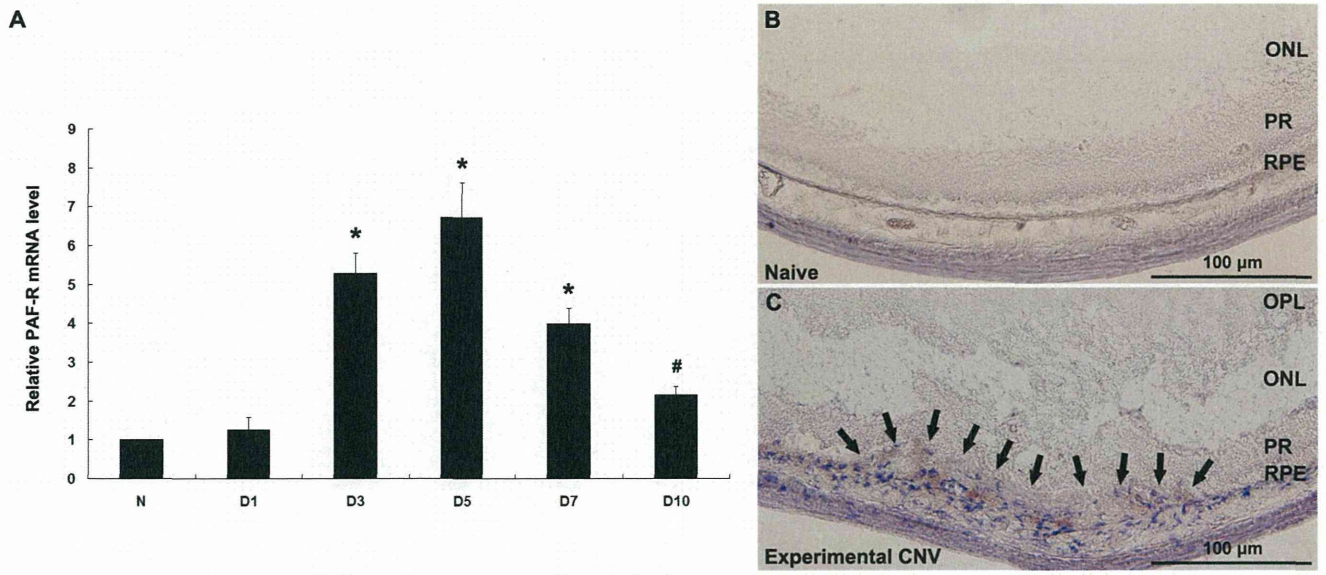

Figure 1. PAF-R expression during laser-induced CNV development. PAF-R mRNA expression in RPE–choroid complexes was determined by qRT-PCR analysis at various time points after photocoagulation (A). *$P<0.01$, #$P<0.05$ compared with the 0-hour baseline. Experiments were conducted in triplicate with similar results. Error bars indicate mean ± SD; n = 6 for each time point. Immunhistochemical analysis of PAF-R was performed in treatment-naïve eye (B) and experimental CNV tissue (arrows) on day 5 after laser treatment (C). Naïve: no laser treatment. OPL: outer plexiform layer; ONL: outer nuclear layer; PR: photoreceptors; RPE: RPE cell layer. Representative images are shown. Scale bars in B and C are 100 μm. Naïve, n = 3, experimental CNV, n = 6.
doi:10.1371/journal.pone.0068173.g001

tissues, including spleen, small intestine, kidney, liver, lung, and brain, and in many cell types, including smooth muscle cells, cardiomyocytes, neutrophils, monocytes/macrophages, eosinophils, endothelial cells, and Kupffer cells [28,29]. In the eye, PAF-R localizes to the corneal epithelium, iris/ciliary body, and retina [30–32] and recently was identified in RPE cells and choroidal endothelial cells [24]. Previous studies have indicated that PAF-R was upregulated during inflammatory processes, cancer progression, and wound healing process [33–35]. To our knowledge, the roles of PAF-R in CNV have not been addressed

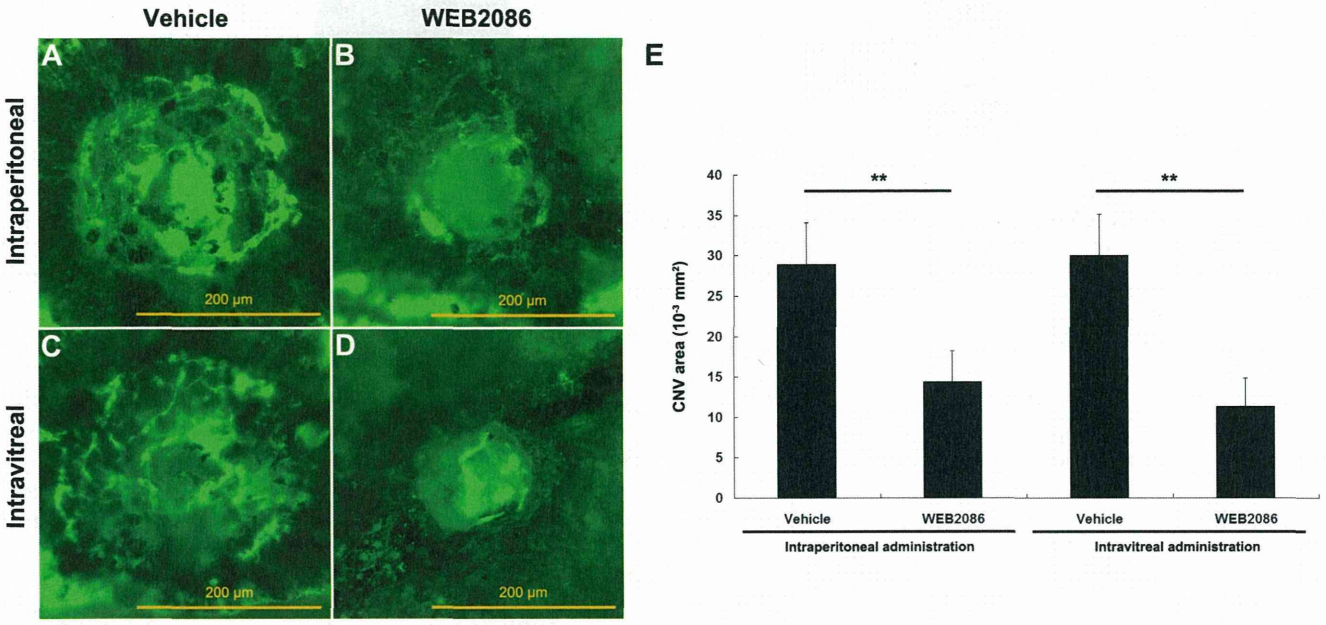

Figure 2. Inhibitory effects of PAF-R blockage on CNV. Representative images of fluorescein dextran perfused RPE–choroidal flat mounts of mice administered PBS vehicle only (A, C), WEB2086 intraperitoneally (B), or WEB2086 intravitreally (D) on day 10 after laser injury. The CNV area was measured quantitatively (E). **$P<0.001$ compared with vehicle-treated mice. Experiments were conducted in triplicate with similar results. Error bars indicate mean ± SD; intraperitoneal vehicle, n = 20, intraperitoneal WEB2086, n = 21, intravitreal vehicle, n = 20, intravitreal WEB2086, n = 22. Scale bars in A–D are 200 μm.
doi:10.1371/journal.pone.0068173.g002

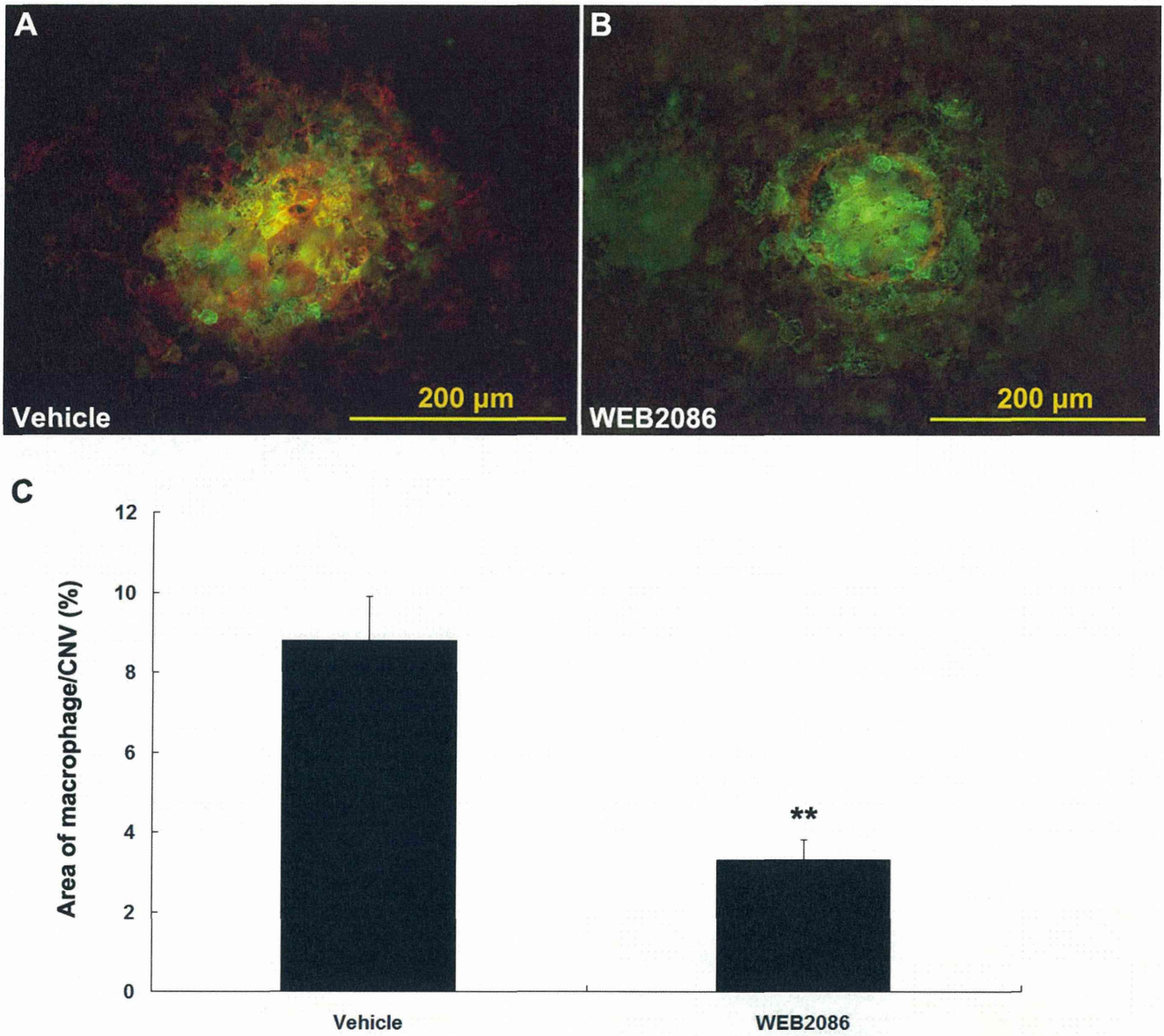

Figure 3. Suppressive effects of PAF-R blockage on macrophage infiltration in CNV. Immunohistochemical analysis of lesions in the choroid of vehicle- (A) or WEB2086-treated (B) mice 72 h after laser treatment. Green fluorescence from isolectin B4 indicates CNV, and red fluorescence indicates F4/80-positive macrophages. The area of F4/80-positive cells was quantified and normalized to the area of CNV (C). $^{**}P<0.001$ compared with vehicle-treated mice. Error bars indicate mean ± SD; vehicle, n = 16, WEB2086, n = 16. Experiments were conducted in triplicate with similar results. Scale bars in A and B are 200 μm.
doi:10.1371/journal.pone.0068173.g003

previously. We report here that PAF-R is upregulated during laser-induced CNV development. Laser photocoagulation is an established method for generating CNV in animal models. High laser energy causes rupture of Bruch's membrane, and, under the influence of various angiogenic factors, an ingrowth of choroidal vessels under the RPE and into the subretinal space takes place. Although in this model, pathogenesis of the neovascularization is different from AMD, formation of CNV is believed to follow the same pattern, and identical angiogenetic factors are expressed by the RPE and endothelial cells [36]. Our observations underscore the possibility that PAF-R signaling is important in CNV.

In the present study, both systemic and local blockage of PAF-R using the novel PAF-R antagonist WEB2086 led to significant CNV suppression. Previous studies have revealed that a PAF-R blockade can inhibit endothelial cell migration and vascular permeability [19,37]. In a corneal micropocket assay, the Matrigel model, and in an experimental tumor model, PAF-R antagonists significantly reduced VEGF-related and tumor-related angiogenesis [18,19,38–40]. WEB2086, a thieno-triazolo-diazepine, is a very potent and specific PAF-R antagonist with an affinity for PAF binding sites that is similar to the affinity of PAF itself [41]. Pharmacological data from animal studies support the possibility of using WEB2086 as a peroral, intravenous, or inhaled PAF-R antagonist at low dosage [41]. However, data are lacking regarding the pharmacological properties, toxicology, and safety profiles associated with intraocular administration of WEB2086. Our results demonstrated that intravitreal administration of WEB2086 inhibits laser-induced CNV without retinal destruction.

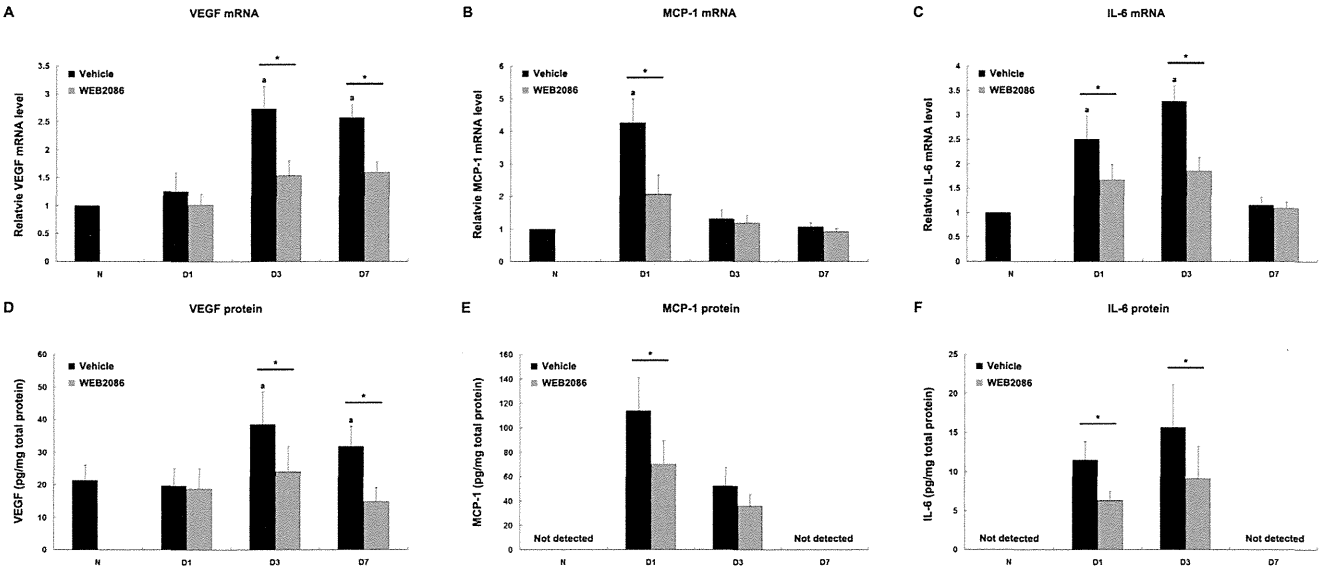

Figure 4. Inhibitory effects of WEB2086 on the expression of proangiogenic and proinflammatory molecules in the RPE-choroid complex. The choroidal mRNA and protein expression levels of VEGF (A, D), MCP-1 (B, E), and IL-6 (C, F) were analyzed by qRT-PCR (A–C) and ELISA (D–F) at various time points after photocoagulation. WEB2086-induced PAF-R blockage significantly suppressed the expression of these molecules, which was upregulated in the vehicle-treated mice during CNV development. *$P<0.01$ compared with vehicle-treated mice, $^{a}P<0.01$ compared with the 0-hour baseline. Error bars indicate mean ± SD; vehicle, n = 8 for each molecule each time point, WEB2086, n = 8 for each molecule each time point. Experiments were conducted in triplicate with similar results.
doi:10.1371/journal.pone.0068173.g004

WEB2086 easily crosses vessel walls and the mucosa of the airways [41], and we speculate that it readily penetrates the retina because of its small molecular weight (456 Da). Further study is necessary to investigate the penetration, intraocular pharmacokinetics, toxicology, and the effects on retinal ultrastructure and function with intravitreal administration of WEB2086. Our results suggest that PAF-R blockage may be a useful strategy in CNV treatment.

Macrophage accumulation in the CNV area and the expression of angiogenic cytokines, such as VEGF, are involved in CNV formation [42–44]. Mice subjected to pharmacological deletion of macrophages exhibited suppressed CNV and reduced VEGF, suggesting a role for macrophages as producers and regulators of angiogenic factors in CNV pathogenesis [45,46]. In the present study, a PAF-R blockade suppressed macrophage infiltration as well as CNV development. Data of our present study are compatible with those of a recent study that observed an inhibition of macrophage infiltration and inflammatory processes following treatment with a PAF-R antagonist or in PAF-R-deficient animal in a model of renal inflammatory injury [47]. These data add to growing evidence supporting the role of chronic inflammatory processes in CNV and suggest that more research is needed to explore the therapeutic potential of anti-inflammatory therapy, such as PAF-R blockage, in AMD.

In addition to VEGF, many other angiogenic and inflammatory mediators contribute to CNV either directly via activation of their cognate receptors or indirectly via crosstalk with VEGF and other signaling pathways [48]. MCP-1, a CC chemoattractant protein, plays an important role in macrophage recruitment and is a key factor in CNV formation following laser injury. Decreased MCP-1 expression is associated with significant inhibition of macrophage infiltration and reduced CNV [49,50]; these features also are observed in CCR2-deficient mice that lack the receptor for MCP-1 [43,51]. IL-6 is a potent proinflammatory cytokine that may function in the pathogeneses of ocular neovascularization, such as proliferative diabetic retinopathy [52]. In experimental CNV, IL-6 expression is upregulated in the RPE–choroid complex, and antibody-based blockage of the IL-6 receptor or genetic ablation of IL-6 significantly suppress CNV [49]. We report that a PAF-R blockade significantly suppressed CNV-related molecules including VEGF, MCP-1, and IL-6. The suppression of VEGF and inflammation-related molecules associated with PAF-R blockage is consistent with the results of other studies that implicated PAF/PAF-R signaling in angiogenesis and inflammatory processes [53–55]. The molecular mechanisms functioning in CNV suppression by PAF-R blockage likely involve the inhibition of multiple inflammatory steps.

It is known that CNV lesions commonly evolve into scars over time as a consequence of the wound healing process. In addition, subretinal fibrosis contributes to a loss in visual acuity in neovascular AMD. A recent study documented the development or progression of submacular fibrosis following anti-VEGF therapy in patients with exudative AMD [56]. In these cases, the vascular component of AMD was treatable with anti-VEGF agents, but the visual outcome was ultimately limited by submacular fibrosis. Greater fibrotic responses after anti-VEGF therapy may result from an imbalance in the complex interactions between angiogenesis and tissue fibrosis during the wound healing process [56]. Ultimately, it is the scarring response that irreversibly damages photoreceptors; therefore, therapies that modify this response may help preserve or even rescue photoreceptors. PAF/PAF-R signaling may be a potential therapeutic target as it is believed to play a critical role in various fibrotic processes. For example, PAF signaling upregulates fibronectin expression and matrix production in tubuloepithelial cells and interstitial fibroblasts, two key cell types associated with renal fibrosis [57]. PAF-R is upregulated in experimental lung and liver fibrosis models, and PAF-R antagonists attenuate fibrotic responses [58–60]. These findings are consistent with our results, suggesting that WEB2086 substantially reduces subretinal fibrosis in a mouse model. As RPE cells, expressing PAF-R, have been identified not only as the

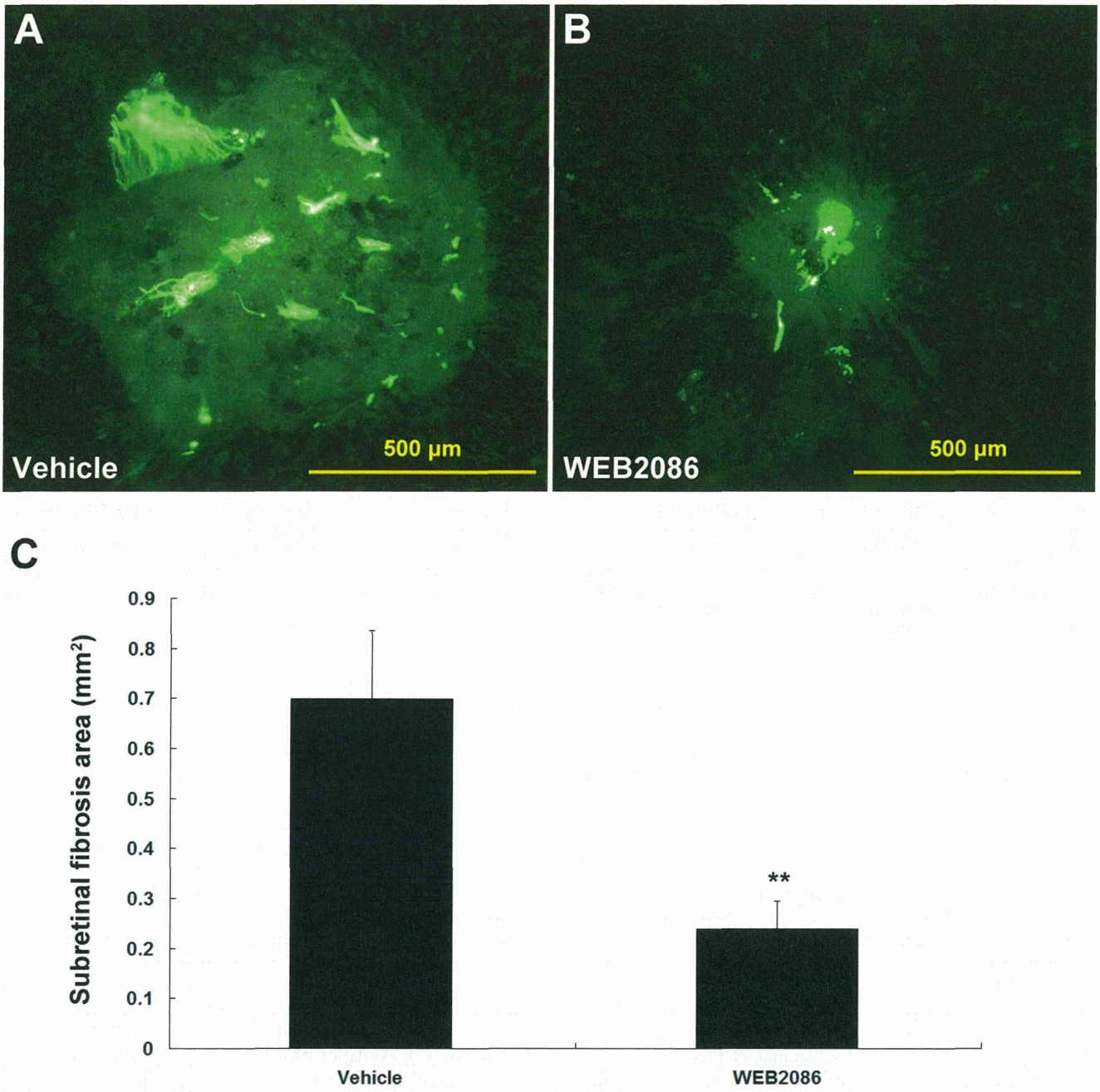

Figure 5. Suppression of subretinal fibrosis with WEB2086-induced PAF-R blockage in a mouse model. Representative subretinal fibrotic scarring of choroidal flat mounts from the vehicle-treated (A) or WEB2086-treated (B) mice 7 days after the induction of subretinal fibrosis. The areas of subretinal fibrosis were evaluated quantitatively by measuring the fluorescence-positive area and compared between the two groups (C). $^{**}P<0.001$ compared with vehicle-treated mice. Error bars indicate mean ± SD; vehicle, n = 20, WEB2086, n = 20. Experiments were conducted in triplicate with similar results. Scale bars in A and B are 500 μm.
doi:10.1371/journal.pone.0068173.g005

central cell type in various ocular wound healing processes but also an important source of transforming growth factor-β, a key molecule, under pathologic conditions [2,61], we hypothesize that they are involved in PAF-R blockage-induced fibrosis suppression in the animal model.

In summary, the present study is the first to demonstrate that PAF-R blockage reduces CNV and subretinal fibrosis *in vivo*. As optimal treatment modalities for neovascular AMD would target the multiple mechanisms of AMD-associated vision loss, including neovascularization, inflammation, and fibrosis, our results support PAF-R as an attractive target in the treatment of AMD, as well ad other ocular wound healing processes, such as proliferative diabetic retinopathy and retinopathy of prematurity.

Acknowledgments

We sincerely thank Ms. Michiyo Takahara for her excellent technical support throughout the experiments. We also thank Ms. Mari Imamura for her help in preparing the histological sections.

Author Contributions

Conceived and designed the experiments: HZ KHS TI. Performed the experiments: HZ AT YY TY YO. Analyzed the data: HZ. Contributed reagents/materials/analysis tools: TI AT TY. Wrote the paper: HZ AT KHS.

References

1. Fine SL, Berger JW, Maguire MG, Ho AC (2000) Age-related macular degeneration. N Engl J Med 342: 483–492.
2. Friedlander M (2007) Fibrosis and diseases of the eye. J Clin Invest 117: 576–586.
3. Kent D, Sheridan C (2003) Choroidal neovascularization: a wound healing perspective. Mol Vis 9: 747–755.
4. Rosenfeld PJ, Shapiro H, Tuomi L, Webster M, Elledge J, et al. (2011) Characteristics of patients losing vision after 2 years of monthly dosing in the phase III ranibizumab clinical trials. Ophthalmology 118: 523–530.
5. Martin DF, Maguire MG, Ying GS, Grunwald JE, Fine SL, et al. (2011) Ranibizumab and bevacizumab for neovascular age-related macular degeneration. N Engl J Med 364: 1897–1908.
6. Rosenfeld PJ, Brown DM, Heier JS, Boyer DS, Kaiser PK, et al. (2006) Ranibizumab for neovascular age-related macular degeneration. N Engl J Med 355: 1419–1431.
7. Brown DM, Kaiser PK, Michels M, Soubrane G, Heier JS, et al. (2006) Ranibizumab versus verteporfin for neovascular age-related macular degeneration. N Engl J Med 355: 1432–1444.
8. Takeda A, Baffi JZ, Kleinman ME, Cho WG, Nozaki M, et al. (2009) CCR3 is a target for age-related macular degeneration diagnosis and therapy. Nature 460: 225–230.
9. Zarbin MA (2004) Current concepts in the pathogenesis of age-related macular degeneration. Arch Ophthalmol 122: 598–614.
10. Grisanti S, Tatar O (2008) The role of vascular endothelial growth factor and other endogenous interplayers in age-related macular degeneration. Prog Retin Eye Res 27: 372–390.
11. Xu H, Chen M, Forrester JV (2009) Para-inflammation in the aging retina. Prog Retin Eye Res 28: 348–368.
12. Fukuda AI, Breuel KF (1996) Effect of platelet activating factor on embryonic development and implantation in the mouse. Hum Reprod 11: 2746–2749.
13. Nilsson G, Metcalfe DD, Taub DD (2000) Demonstration that platelet-activating factor is capable of activating mast cells and inducing a chemotactic response. Immunology 99: 314–319.
14. Braquet P, Paubert-Braquet M, Bourgain RH, Bussolino F, Hosford D (1989) PAF/cytokine auto-generated feedback networks in microvascular immune injury: consequences in shock, ischemia and graft rejection. J Lipid Mediat 1: 75–112.
15. Kasperska-Zajac A, Brzoza Z, Rogala B (2008) Platelet activating factor as a mediator and therapeutic approach in bronchial asthma. Inflammation 31: 112–120.
16. Honda Z, Ishii S, Shimizu T (2002) Platelet-activating factor receptor. J Biochem 131: 773–779.
17. Camussi G, Montrucchio G, Lupia E, De Martino A, Perona L, et al. (1995) Platelet-activating factor directly stimulates in vitro migration of endothelial cells and promotes in vivo angiogenesis by a heparin-dependent mechanism. J Immunol 154: 6492–6501.
18. Ma X, Ottino P, Bazan HE, Bazan NG (2004) Platelet-activating factor (PAF) induces corneal neovascularization and upregulates VEGF expression in endothelial cells. Invest Ophthalmol Vis Sci 45: 2915–2921.
19. Montrucchio G, Lupia E, Battaglia E, Del Sorbo L, Boccellino M, et al. (2000) Platelet-activating factor enhances vascular endothelial growth factor-induced endothelial cell motility and neoangiogenesis in a murine matrigel model. Arterioscler Thromb Vasc Biol 20: 80–88.
20. Ko HM, Seo KH, Han SJ, Ahn KY, Choi IH, et al. (2002) Nuclear factor kappaB dependency of platelet-activating factor-induced angiogenesis. Cancer Res 62: 1809–1814.
21. Cohen RA, Gebhardt BM, Bazan NG (1994) A platelet-activating factor antagonist reduces corneal allograft inflammation and neovascularization. Curr Eye Res 13: 139–144.
22. Montrucchio G, Lupia E, Battaglia E, Passerini G, Bussolino F, et al. (1994) Tumor necrosis factor alpha-induced angiogenesis depends on in situ platelet-activating factor biosynthesis. J Exp Med 180: 377–382.
23. Camussi G, Montrucchio G, Lupia E, Soldi R, Comoglio PM, et al. (1997) Angiogenesis induced in vivo by hepatocyte growth factor is mediated by platelet-activating factor synthesis from macrophages. J Immunol 158: 1302–1309.
24. He YG, Wang H, Zhao B, Hsu M, Liao D, et al. (2009) Functional analysis of platelet-activating factor in the retinal pigment epithelial cells and choroidal endothelial cells. Curr Eye Res 34: 957–965.
25. Zhang H, Sonoda KH, Hijioka K, Qiao H, Oshima Y, et al. (2009) Antiangiogenic immunotherapy targeting Flk-1, DNA vaccine and adoptive T cell transfer, inhibits ocular neovascularization. Biochem Biophys Res Commun 381: 471–476.
26. Jo YJ, Sonoda KH, Oshima Y, Takeda A, Kohno R, et al. (2011) Establishment of a new animal model of focal subretinal fibrosis that resembles disciform lesion in advanced age-related macular degeneration. Invest Ophthalmol Vis Sci 52: 6089–6095.
27. Izumi T, Shimizu T (1995) Platelet-activating factor receptor: gene expression and signal transduction. Biochim Biophys Acta 1259: 317–333.
28. Bito H, Honda Z, Nakamura M, Shimizu T (1994) Cloning, expression and tissue distribution of rat platelet-activating-factor-receptor cDNA. Eur J Biochem 221: 211–218.
29. Montrucchio G, Alloatti G, Camussi G (2000) Role of platelet-activating factor in cardiovascular pathophysiology. Physiol Rev 80: 1669–1699.
30. Domingo MT, Chabrier PE, Van Delft JL, Verbeij NL, Van Haeringen NJ, et al. (1989) Characterization of specific binding sites for PAF in the iris and ciliary body of rabbit. Biochem Biophys Res Commun 160: 250–256.
31. Thierry A, Doly M, Braquet P, Cluzel J, Meyniel G (1989) Presence of specific platelet-activating factor binding sites in the rat retina. Eur J Pharmacol 163: 97–101.
32. Mori M, Aihara M, Shimizu T (1997) Localization of platelet-activating factor receptor messenger RNA in the rat eye. Invest Ophthalmol Vis Sci 38: 2672–2678.
33. Yang HH, Pang JH, Hung RY, Chau LY (1997) Transcriptional regulation of platelet-activating factor receptor gene in B lymphoblastoid Ramos cells by TGF-beta. J Immunol 158: 2771–2778.
34. Aponte M, Jiang W, Lakkis M, Li MJ, Edwards D, et al. (2008) Activation of platelet-activating factor receptor and pleiotropic effects on tyrosine phospho-EGFR/Src/FAK/paxillin in ovarian cancer. Cancer Res 68: 5839–5848.
35. Ma X, Bazan HE (2000) Increased platelet-activating factor receptor gene expression by corneal epithelial wound healing. Invest Ophthalmol Vis Sci 41: 1696–1702.
36. Semkova I, Peters S, Welsandt G, Janicki H, Jordan J, et al. (2003) Investigation of laser-induced choroidal neovascularization in the rat. Invest Ophthalmol Vis Sci 44: 5349–5354.
37. Sirois MG, Edelman ER (1997) VEGF effect on vascular permeability is mediated by synthesis of platelet-activating factor. Am J Physiol 272: H2746–2756.
38. Montrucchio G, Sapino A, Bussolati B, Ghisolfi G, Rizea-Savu S, et al. (1998) Potential angiogenic role of platelet-activating factor in human breast cancer. Am J Pathol 153: 1589–1596.
39. Bussolino F, Arese M, Montrucchio G, Barra L, Primo L, et al. (1995) Platelet activating factor produced in vitro by Kaposi's sarcoma cells induces and sustains in vivo angiogenesis. J Clin Invest 96: 940–952.
40. Robert EG, Hunt JD (2001) Lipid messengers as targets for antiangiogenic therapy. Curr Pharm Des 7: 1615–1626.
41. Casals-Stenzel J, Muacevic G, Weber KH (1987) Pharmacological actions of WEB 2086, a new specific antagonist of platelet activating factor. J Pharmacol Exp Ther 241: 974–981.
42. Ishibashi T, Hata Y, Yoshikawa H, Nakagawa K, Sueishi K, et al. (1997) Expression of vascular endothelial growth factor in experimental choroidal neovascularization. Graefes Arch Clin Exp Ophthalmol 235: 159–167.
43. Tsutsumi C, Sonoda KH, Egashira K, Qiao H, Hisatomi T, et al. (2003) The critical role of ocular-infiltrating macrophages in the development of choroidal neovascularization. J Leukoc Biol 74: 25–32.
44. Grossniklaus HE, Ling JX, Wallace TM, Dithmar S, Lawson DH, et al. (2002) Macrophage and retinal pigment epithelium expression of angiogenic cytokines in choroidal neovascularization. Mol Vis 8: 119–126.
45. Espinosa-Heidmann DG, Suner IJ, Hernandez EP, Monroy D, Csaky KG, et al. (2003) Macrophage depletion diminishes lesion size and severity in experimental choroidal neovascularization. Invest Ophthalmol Vis Sci 44: 3586–3592.
46. Sakurai E, Anand A, Ambati BK, van Rooijen N, Ambati J (2003) Macrophage depletion inhibits experimental choroidal neovascularization. Invest Ophthalmol Vis Sci 44: 3578–3585.
47. Doi K, Okamoto K, Negishi K, Suzuki Y, Nakao A, et al. (2006) Attenuation of folic acid-induced renal inflammatory injury in platelet-activating factor receptor-deficient mice. Am J Pathol 168: 1413–1424.
48. Ding X, Patel M, Chan CC (2009) Molecular pathology of age-related macular degeneration. Prog Retin Eye Res 28: 1–18.
49. Izumi-Nagai K, Nagai N, Ozawa Y, Mihara M, Ohsugi Y, et al. (2007) Interleukin-6 receptor-mediated activation of signal transducer and activator of transcription-3 (STAT3) promotes choroidal neovascularization. Am J Pathol 170: 2149–2158.
50. Nagai N, Oike Y, Izumi-Nagai K, Urano T, Kubota Y, et al. (2006) Angiotensin II type 1 receptor-mediated inflammation is required for choroidal neovascularization. Arterioscler Thromb Vasc Biol 26: 2252–2259.
51. Tsutsumi-Miyahara C, Sonoda KH, Egashira K, Ishibashi M, Qiao H, et al. (2004) The relative contributions of each subset of ocular infiltrated cells in experimental choroidal neovascularisation. Br J Ophthalmol 88: 1217–1222.
52. Funatsu H, Yamashita H, Noma H, Mimura T, Nakamura S, et al. (2005) Aqueous humor levels of cytokines are related to vitreous levels and progression

of diabetic retinopathy in diabetic patients. Graefes Arch Clin Exp Ophthalmol 243: 3–8.
53. Kim HA, Seo KH, Kang YR, Ko HM, Kim KJ, et al. (2011) Mechanisms of platelet-activating factor-induced enhancement of VEGF expression. Cell Physiol Biochem 27: 55–62.
54. Ogata M, Nandate K, Kawasaki T, Kawasaki C, Ozaki M, et al. (2004) A platelet activating factor receptor antagonist inhibits cytokine production in human whole blood by bacterial toxins and live bacteria. Anesth Analg 98: 1767–1772.
55. Proudfoot JM, Croft KD, Puddey IB, Beilin LJ (2003) Angiotensin II type 1 receptor antagonists inhibit basal as well as low-density lipoprotein and platelet-activating factor-stimulated human monocyte chemoattractant protein-1. J Pharmacol Exp Ther 305: 846–853.
56. Hwang JC, Del Priore LV, Freund KB, Chang S, Iranmanesh R (2011) Development of subretinal fibrosis after anti-VEGF treatment in neovascular age-related macular degeneration. Ophthalmic Surg Lasers Imaging 42: 6–11.
57. Ruiz-Ortega M, Bustos C, Plaza JJ, Egido J (1998) Overexpression of extracellular matrix proteins in renal tubulointerstitial cells by platelet-activating-factor stimulation. Nephrol Dial Transplant 13: 886–892.
58. Giri SN, Sharma AK, Hyde DM, Wild JS (1995) Amelioration of bleomycin-induced lung fibrosis by treatment with the platelet activating factor receptor antagonist WEB 2086 in hamsters. Exp Lung Res 21: 287–307.
59. Chen J, Ziboh V, Giri SN (1997) Up-regulation of platelet-activating factor receptors in lung and alveolar macrophages in the bleomycin-hamster model of pulmonary fibrosis. J Pharmacol Exp Ther 280: 1219–1227.
60. Yang Y, Nemoto EM, Harvey SA, Subbotin VM, Gandhi CR (2004) Increased hepatic platelet activating factor (PAF) and PAF receptors in carbon tetrachloride induced liver cirrhosis. Gut 53: 877–883.
61. Holtkamp GM, Kijlstra A, Peek R, de Vos AF (2001) Retinal pigment epithelium-immune system interactions: cytokine production and cytokine-induced changes. Prog Retin Eye Res 20: 29–48.

Jpn J Ophthalmol
DOI 10.1007/s10384-013-0300-6

THE OFFICIAL INTERNATIONAL JOURNAL OF THE JAPANESE OPHTHALMOLOGICAL SOCIETY

CLINICAL INVESTIGATION

Autoantibodies to transient receptor potential cation channel, subfamily M, member 1 in a Japanese patient with melanoma-associated retinopathy

Yukiko Morita · Kazuhiro Kimura · Youichiro Fujitsu · Atsushi Enomoto · Shinji Ueno · Mineo Kondo · Koh-Hei Sonoda

Received: 23 May 2013 / Accepted: 3 December 2013

Abstract
Purpose To report a case of melanoma-associated retinopathy (MAR) in a Japanese patient found to have autoantibodies to transient receptor potential cation channel, subfamily M, member 1 (TRPM1).
Case An 82-year-old man presented with blurred vision OS as well as night blindness and photopsia OU. Fundus photography, fluorescein angiography, and spectral domain-optical coherence tomography findings were essentially normal. Goldmann perimetry revealed a relative central scotoma, including the blind spot in the right eye, as well as a relative scotoma around a blind spot OS. The full-field scotopic electroretinograms showed a "negative-type" pattern OU, suggestive of extensive bipolar cell dysfunction. Systemic examination revealed that the patient had malignant melanoma of the anus with lung metastasis. Autoantibodies to TRPM1 were detected in the serum of the patient by immunoblot analysis. Vitreous opacity developed during follow-up. The visual symptoms and vitreous opacity of the patient were markedly improved after oral prednisolone therapy. The patient died as a result of widespread metastasis of the melanoma at 11 months after his first visit.
Conclusion The present case is the first reported instance of MAR positive for autoantibodies to TRPM1 in an Asian patient.

Keywords Melanoma-associated retinopathy · Electroretinogram (ERG) · Transient receptor potential cation channel, subfamily M, member 1 (TRPM1) · Paraneoplastic retinopathy

Y. Morita · K. Kimura (✉) · Y. Fujitsu · K.-H. Sonoda
Department of Ophthalmology, Yamaguchi University Graduate School of Medicine, 1-1-1 Minami-Kogushi, Ube, Yamaguchi 755-8505, Japan
e-mail: k.kimura@yamaguchi-u.ac.jp

A. Enomoto
Department of Pathology, Nagoya University Graduate School of Medicine, Nagoya, Japan

S. Ueno
Department of Ophthalmology, Nagoya University Graduate School of Medicine, Nagoya, Japan

M. Kondo
Department of Ophthalmology, Mie University Graduate School of Medicine, Tsu, Japan

Introduction

Melanoma-associated retinopathy (MAR) is a paraneoplastic autoimmune manifestation of melanoma that is characterized by various visual signs and symptoms including night blindness, photopsia, visual field defects, and abnormal color vision [1–8]. Patients with MAR also have characteristic electroretinograms (ERGs). The scotopic full-field ERG elicited by a bright flash stimulus shows a "negative-type" pattern with an a-wave of normal amplitude and a b-wave smaller than the a-wave [1–6], suggesting that in MAR patients, the retinal bipolar cells are affected. Historically, autoantibodies to bipolar cells have been recognized as markers of MAR, but the specific bipolar cell antigen has not been identified [8–12].

We and others recently identified autoantibodies specific for transient receptor potential cation channel, subfamily M, member 1 (TRPM1) in the serum of MAR patients [13, 14]. TRPM1 is specifically expressed in retinal ON bipolar cells and functions as a component of the transduction channel in these cells [15–17]. All four MAR

Published online: 29 January 2014

patients with autoantibodies to TRPM1 in these previous reports were Caucasian [13, 14], and individuals with TRPM1-related MAR have not been described for other ethnic groups. Malignant melanoma is rare in the Japanese population, with a prevalence of only 0.002 %, compared with a frequency of 0.015 % in white populations.

We now report a case of MAR positive for serum autoantibodies to TRPM1 in a Japanese individual with melanoma of the anus and metastasis to the lung.

Case report

An 82-year-old man visited Yamaguchi University Hospital with complaints of blurred vision OS as well as night blindness and photopsia OU with a duration of about 1 month. He had not recently been diagnosed with any ocular or systemic disease, including any malignant tumors. His family history revealed no members with any eye diseases. Our initial examination found that his best corrected visual acuity (BCVA) was 1.2 OD and 0.6 OS. Slit-lamp assessment, intraocular pressure measurement, fundus examination, and fluorescein angiography findings were essentially normal OU (Fig. 1a, b). Spectral domain-optical coherence tomography (SD-OCT) (Cirrus HD-OCT; Carl Zeiss Meditec, Dublin, CA, USA) revealed a normal macular structure, with the exception of a slight irregularity of the retinal pigment epithelium in both eyes (Fig. 1c). The thickness of the parafoveal nasal inner nuclear layer (INL) was 40 μm OD and 36 μm OS. Given that the normal thickness of the parafoveal nasal INL was previously determined to be ~40 μm [18], there did not appear to be any thinning of the INL in this patient.

Goldmann perimetry revealed that the visual fields manifested general depression OU. A relative central scotoma including a blind spot was detected OD, and a relative scotoma around the blind spot was detected OS, with the I-4e target (Fig. 2a). Color vision tested with Ishihara color plates was normal, but the Standard Pseudoisochromatic Plates part 2 (SPP-2) test and the panel D-15 test revealed a mild blue-yellow defect OS. A dark-adaptation test revealed a poorly defined red-cone break and elevated threshold level, with a log threshold (arbitrary units) value of 6 after 40 min. Full-field ERGs were recorded with a bright flash stimulus of 20 J after 20 min of dark adaptation. They showed a normal a-wave and a b-wave with a markedly reduced amplitude, giving rise to a "negative-type" pattern OU (Fig. 2b).

On the basis of these ophthalmological and electrophysiological findings, we tentatively diagnosed the patient with paraneoplastic retinopathy and performed systemic examinations. Whole-body computed tomography (CT) revealed a tumor in his right lung (Fig. 2c). Biopsy specimens were obtained from a hilar lymph node in the right lung by bronchoscopy, and histology revealed the mass to be a malignant melanoma (Fig. 2d). Positron emission tomography was performed, but the site of the primary tumor was not identified. There was physiological accumulation of the tracer in the bladder. We consulted a dermatologist, and the patient was then treated with DAV-Feron (dacarbazine, nimustine hydrochloride, vincristine, and interferon-β) chemotherapy. His BCVA remained at 1.0 OD and 0.7 OS, but vitreous opacity appeared OS and perimetry revealed enlarged blind spots OU.

Given that autoantibodies to TRPM1 have been detected in patients with paraneoplastic retinopathy associated with dysfunction of retinal ON bipolar cells [13, 14], we examined whether such autoantibodies were also present in the serum of our MAR patient. Immunoblot analysis revealed that serum from the patient yielded a pronounced immunoreactive band with lysates of cells transfected with an expression vector for human TRPM1 (Fig. 3). Negative control serum did not show such reactivity. These results suggested that the serum of the proband contained autoantibodies to TRPM1.

The patient received oral prednisolone at 40 mg/day for treatment of his MAR. Four weeks after the onset of prednisolone therapy, the vitreous opacity had disappeared and the blind spot enlargement was markedly attenuated OU. Four months after his initial visit, the patient was diagnosed with anal malignant melanoma, with the late diagnosis being attributable to the misidentification of his anal tumor as a hemorrhoid. The lung tumor was thus likely a metastasis from anal malignant melanoma. The patient died at 11 months after his first visit as a result of metastasis to the brain, lung, liver, bilateral hilar lymph nodes, mediastinal lymph nodes, and inguinal lymph nodes.

Discussion

The patient presented with blurred vision, night blindness, and photopsia associated with a "negative-type" ERG, indicative of dysfunction of retinal bipolar cells. Systemic examination revealed malignant melanoma in the lung and anus. The serum of the patient was also positive for autoantibodies to TRPM1. On the basis of these findings, we diagnosed the patient with MAR likely caused by autoantibodies to TRPM1. Only four patients with TRPM1-related MAR have been reported to date, all of whom were Caucasian [13, 14]. The present Japanese patient thus represents the first case of TRPM1-related MAR in an ethnic group other than Caucasian. Our findings suggest that autoantibodies to TRPM1 may play an important role in the pathogenesis of MAR regardless of ethnicity.

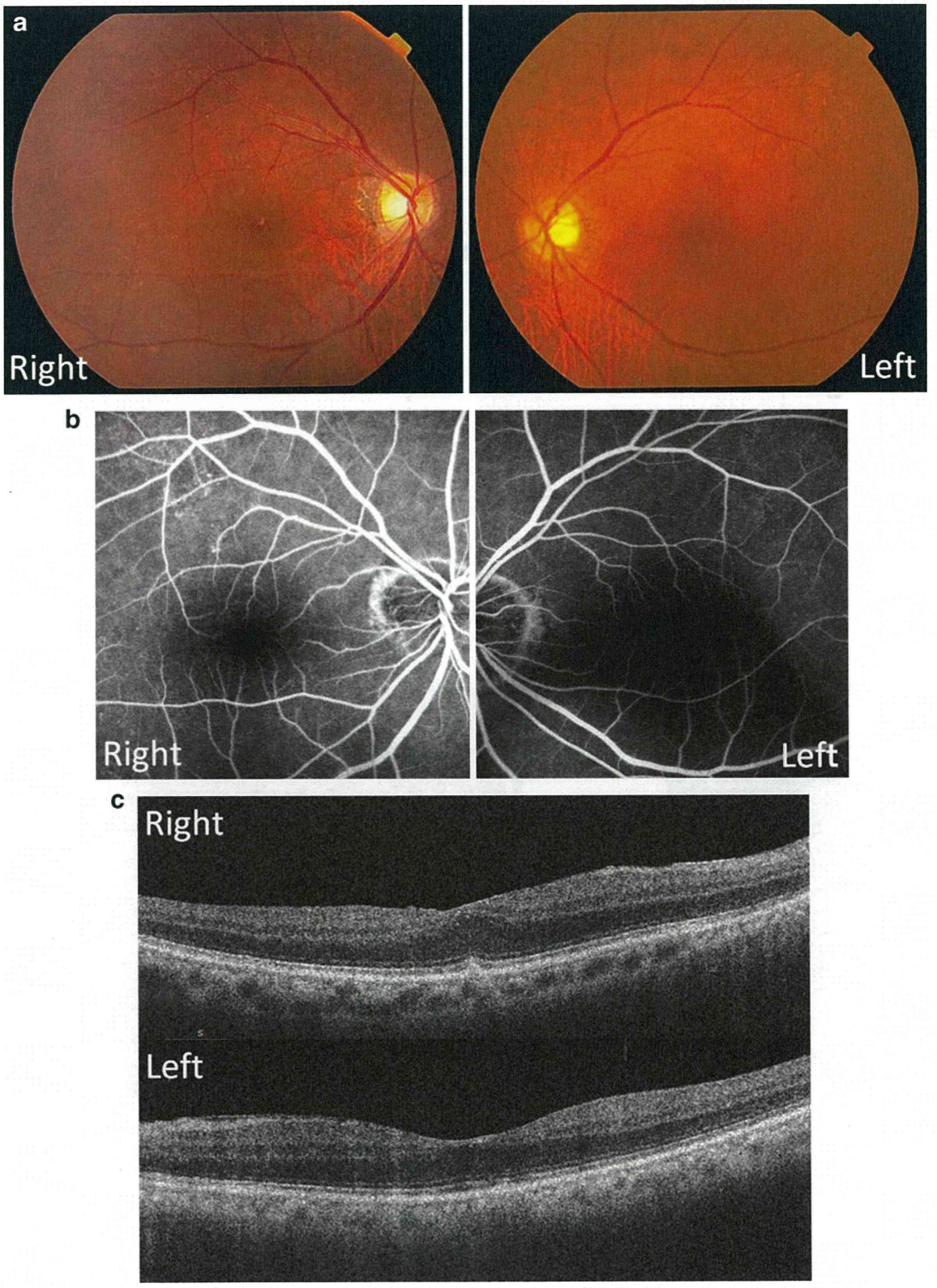

Fig. 1 Fundus photography, fluorescein angiography, and SD-OCT performed at the initial visit of the patient. **a** Fundus photographs revealed no abnormality in either eye. **b** Fundus fluorescence angiography revealed no abnormality in either eye. **c** Spectral domain-optical coherence tomography (SD-OCT) images for a 6-mm horizontal scan of the retina were essentially normal, with the exception of a slight irregularity of the retinal pigment epithelium in both eyes